Advances in Material Research and Technology

Nithyadharseni Palaniyandy
K. P. Abhilash
B. Nalini *Editors*

Solid State Batteries

Design, Challenges and Market Demands

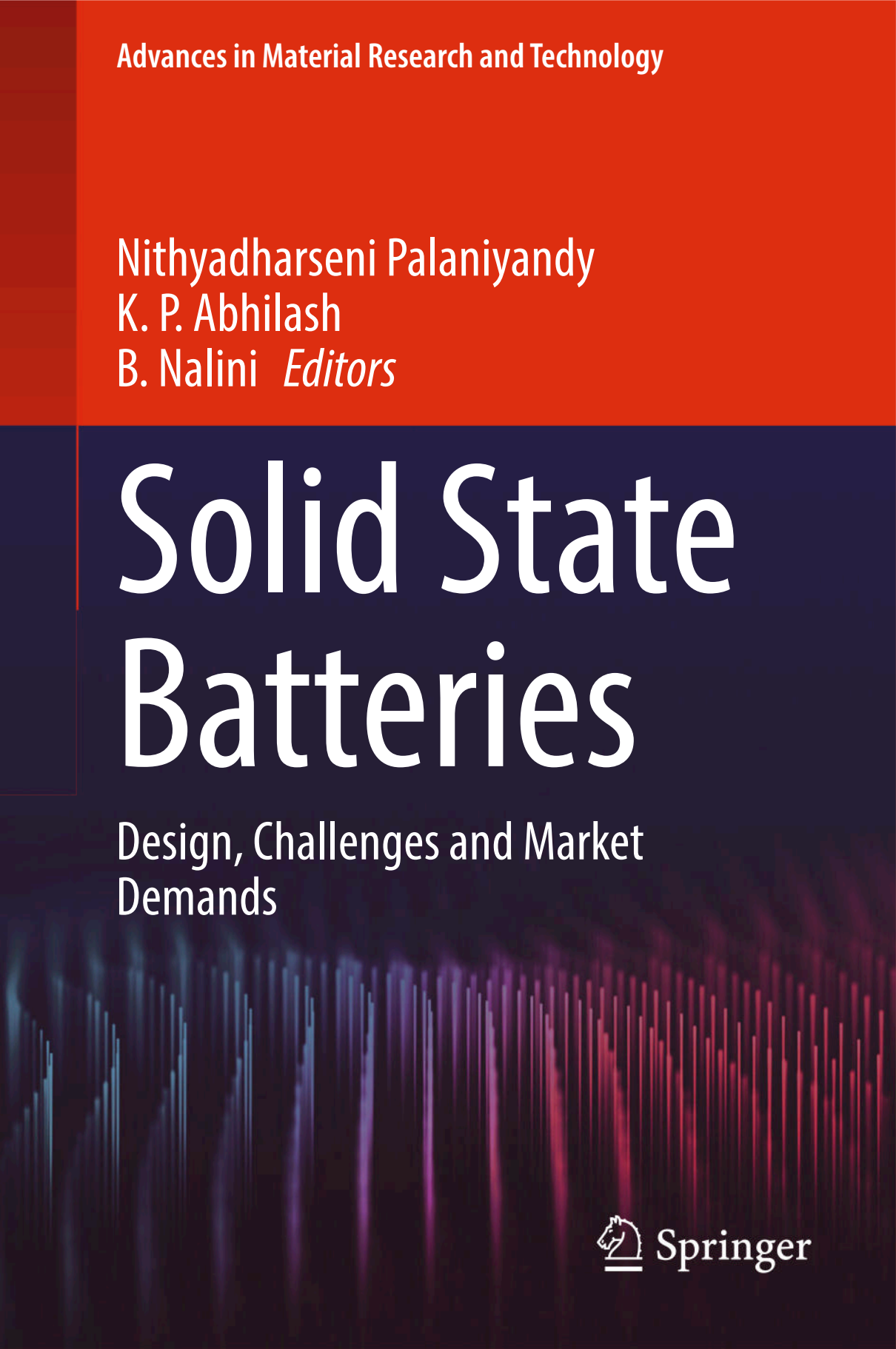

Springer

Advances in Material Research and Technology

This Series covers the advances and developments in a wide range of materials such as energy materials, optoelectronic materials, minerals, composites, alloys and compounds, polymers, green materials, semiconductors, polymers, glasses, nanomaterials, magnetic materials, superconducting materials, high temperature materials, environmental materials, Piezoelectric Materials, ceramics, and fibers.

Nithyadharseni Palaniyandy · K. P. Abhilash ·
B. Nalini
Editors

Solid State Batteries

Design, Challenges and Market Demands

Springer

Editors
Nithyadharseni Palaniyandy
Institute for the Development of Energy
for African Sustainability (IDEAS)
College of Science, Engineering,
and Technology (CSET)
University of South Africa
Roodepoort, South Africa

B. Nalini
Avinashilingam Institute for Home Science
and Higher Education for Women
Coimbatore, India

K. P. Abhilash
Department of Inorganic Chemistry
University of Chemistry and Technology
Prague, Czech Republic

ISSN 2662-4761 ISSN 2662-477X (electronic)
Advances in Material Research and Technology
ISBN 978-3-031-12469-3 ISBN 978-3-031-12470-9 (eBook)
https://doi.org/10.1007/978-3-031-12470-9

This Springer imprint is published by the registered company Springer Nature Switzerland AG
The registered company address is: Gewerbestrasse 11, 6330 Cham, Switzerland

Preface

The demand for alternative power sources for perceiving sustainable/clean energy has created an increasing interest and has become more critical owing to the development of applications such as electric vehicles and new types of portable electronic devices, currently emerging in the market. In order to get LIBs ready for large-scale implementation in Heavy Electric Vehicles (HEVs), researchers tend to improvise or troubleshoot several aspects that connect to performance, stability, safety, and feasibility of large-scale production. Emphasize on all aspects of single electrochemical cells such as novel electrolytes, electrodes, methods to improve the energy/power density, development of high-performance conductive additives/current collectors, efficient packaging, and so on are made. In this realm, among the different battery design strategies, all-solid-state assembly is the promising approach towards the safest technology, giving high energy/power density and reduction in running cost of manufacturing in the growing electronic world. One of the major hindrances or barriers in all-solid-state assembly is the non-availability of in-depth literature to cover from its design strategy to the challenges to be addressed in terms of its interfaces and electrodes. Consolidating the scattered literatures available and analyzing the results on all-solid-state lithium batteries will be the most valid approach to drivel this arena forward to the stage of mellowness and thus to naturalization which is the purpose of this book.

The book offers a comprehensive analysis of the principle, Physical, Chemical, and Electrochemical backgrounds and novel design strategies and waste management in higher energy solid-state lithium batteries. This addresses different subdivisions of energy devices such as battery science, energy storage, electrochemical device, and nanotechnology in energy. The book also covers the information on synthesis and experimental techniques and characterization of physical, chemical, and electrochemical properties of the electrodes and electrolytes. The major lacking point in most of the available literature and books is the precise descriptions of the electrochemical measurements of conductivity and related parameters in solid electrolytes and their interfaces, which will be one of the major highlights of this book. It reviews the recent progress and trends of the materials (electrodes and electrolytes), additive

manufacturing technology, and so on for the production of solid-state battery with special consideration for its cost and the market needs.

The major highlights of the book include but not limited to the areas such as novel design strategies of all-solid-state assemblies, state of the art of novel electrodes and electrolytes for all-solid-state batteries, solid-solid interfaces and related challenges in all-solid-state batteries, and current situation and the features to be improved in all-solid-state batteries. The book also provides insight into the present-day market scenario on (i) the demand and supply, (ii) the technology of all-solid-state lithium-ion batteries and their applications in different energy fields, (iii) narrates various technologies involved such as thin-film, 3D printing (additive manufacturing), atomic layer deposition, and (iv) other recent strategies that have been used for the fabrication of all-solid-state lithium-ion batteries. The description of the complete functioning and challenges with the electrochemistry of the electrodes and solid electrolyte interfaces has been included as a major part in this book. The book also supplies valuable insight into potential growth opportunities in this exciting market and cost-effective design tactics in all-solid-state assemblies. The book caters the knowledge quotient of not only the pursuing scientists but also the budding researchers say, graduate students working on batteries, engineers, and technologists who want a compendium that consolidates knowledge from the fundamentals of battery science to commercialization aspects that demands intradisciplinary understanding regarding the interaction of electrochemistry, solid-state materials science and surfaces and interfaces.

Roodepoort, South Africa — Nithyadharseni Palaniyandy
Prague, Czech Republic — K. P. Abhilash
Coimbatore, India — B. Nalini

Contents

Chapter 1
Basic Aspects of Design and Operation of All-Solid-State Batteries

P. Priyanka, B. Nalini, and P. Nithyadharseni

1.1 Introduction

Portable electronics, automobile sectors and grid-scale storage systems have revolutionized today's world and battery technology plays a vital role in bringing out the key aspects of energy storage and supply. Commercially, Lithium-ion Batteries (LIBs) have been considered to be the hopeful solution in meeting the demand for energy storage systems. In the present commercial batteries, the electrolyte used is 1 M $LiPF_6$ in EC-DMC at 27 °C which has got excellent conductivity of 12 mS/cm which is the goal set for solid-state electrolyte if one wants to replace the present-day batteries with all-solid-state batteries [1]. The electrolyte used in LIBs exist as a liquid, either aqueous/non-aqueous. The use of liquid electrolytes in the traditional LIBs with the presence of organic solvents cause issues on safety problems, thermal runaway and risk of leakage of electrolyte which in turn leads to short circuit and failure of the battery [1].

In 2016, 92 Samsung Note 7 cell phones caught fire which resulted in a large product recall [2]. Notebook computers [2, 3], hoverboards [3] and other Li-ion battery-powered gadgets have also been referenced in fire-related accidents. These accidents are more prone due to the dendrite formation in batteries. The interfacial dendrites formed on the anode create the possibility of an internal short circuit, catching fire and even explosion [4]. The highly flammable nature of the liquid electrolyte leads to dangerous or disastrous consequences due to the leakage

P. Priyanka · B. Nalini (✉)
Department of Physics, Avinashilingam Institute for Home Science and Higher Education for Women, Tamil Nadu, Coimbatore 641043, India
e-mail: nalini_phy@avinuty.ac.in; jyothsnalalin99@gmail.com

P. Nithyadharseni
Institute for the Development of Energy for African Sustainability (IDEAS), College of Science, Engineering, and Technology, University of South Africa, Florida Science Campus, Roodepoort 1709, South Africa
e-mail: Palann@unisa.ac.za

N. Palaniyandy et al. (eds.), *Solid State Batteries*, Advances in Material Research and Technology, https://doi.org/10.1007/978-3-031-12470-9_1

or rupturing in automobile crashes. To alleviate these challenges, All-Solid-State Batteries (ASSBs) comes into play which replaces organic liquid electrolytes with a solid electrolyte. Thermal runaway can be avoided by replacing the flammable liquid electrolytes with a solid electrolyte. ASSBs are not only good at improvising safety but also have a lot of capacity and stability. New-age lithium solid-state batteries are challenging the predominance of traditional liquid electrolyte-based batteries as developments in solid-state batteries reach commercial promise. Solid-state batteries are 80–90% thinner and have a higher decomposition voltage than lithium batteries. As a result, the gravimetric energy density can be increased and the increased energy density will result in higher power output, which will improve all electronic devices significantly [5].

Marching towards the next-generation energy storage technology of electric vehicles (EVs), the global market widely depends on the solid-state batteries with energy density >450 Wh/Kg. Researchers have been working for more than three decades to identify various solid electrolytes in the domains of electrochemistry, material science, polymer chemistry and other fields. Still, the number of feasible solid electrolytes exhibiting high ionic conductivity is inadequate. The incompatibility of these materials with other components of the system, such as electrodes, is one of their intrinsic limits. The close contact between these liquid electrolytes and electrodes is a rate-limiting concern in real systems. Solid electrolytes, when chosen compatible with either electrode, would improve the energy density of the battery. In addition, the advantages of thinner electrolyte and compact packaging can be reaped. Though the use of lithium metal as a negative electrode might double the cell's energy density, it is desirable to achieve the expected performance with lithium alloys or non-lithium alloys too [6].

The fabrication of all-solid-state batteries includes processing techniques such as printing, pressing, calendaring, etc. Each method has its own set of advantages and disadvantages, which are also described. The need for solid-state battery technology with the identification of good electrode/electrolytes is the major counterpart. Although ASSBs have many advantages over commercial LIBs, their development with commercial viability is limited. Researchers are aiming at this technology for a power-packed future with practicability in the industries which could also satisfy the demand for energy storage, especially in the field of electric vehicles. In this chapter, the different design of battery technology with the processing techniques of SSBs and their interfacial development as full cell is discussed.

1.2 Battery Design

A conventional lithium-ion battery comprises of the basic components, anode and cathode immersed in an electrolyte and separated by a separator membrane as shown in Fig. 1.1a. In solid-state batteries, separator and electrolytes are made into one unit since the electrolyte itself would act as both separator and electrolyte. However, in a semi-solid battery where polymer electrolytes are used, the polymer membranes

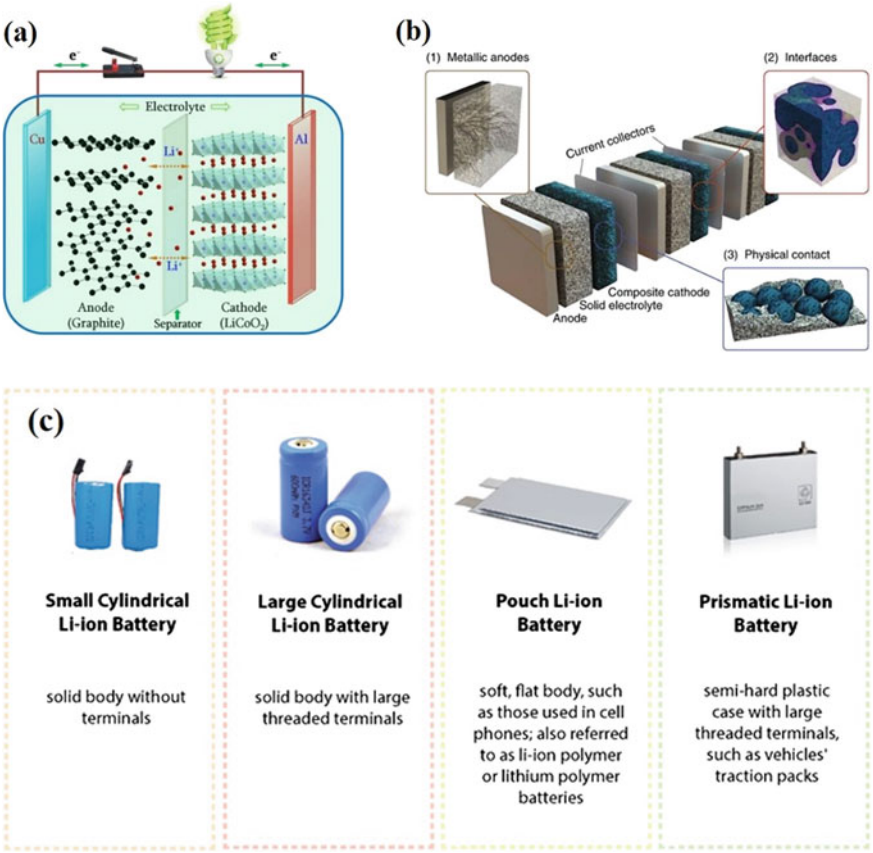

Fig. 1.1 **a** Schematic representation of LIBs [7], **b** All-solid-state batteries [8] and **c** Different shapes of batteries [9]

are tailored with conducting salt fillers to achieve the performance of the electrolyte. Hence, every all-solid-state battery would have essentially three components say an anode, a cathode and an electrolyte.

Operation of Batteries

Solid-state batteries involve a chemistry with redox processes to store and deliver energy. An electrically conductive substance is used to make these two electrodes. An electrolyte containing electrically charged particles is present between these two electrodes. Lithium ions can move through the electrolyte and interact with the anode or cathode (depending on charging or discharging). The transfer of electrical charge between the cathode and anode (through a circuit) is enabled by this chemical process, allowing a battery to generate an electric current to power any gadget.

The anode undergoes oxidation, while the cathode undergoes reduction, and the battery can exploit this occurrence to store (charge) and release (discharge) energy

as needed. In case of an ordinary liquid electrolyte, the saturated ionic salt in solvent offers the mobility of ions, whereas, in the solid electrolyte, ions move through an ion-conductive solid matrix. Figure 1.1b shows the schematic diagram of ASSBs with the major parts and it also shows the challenges faced by ASSBs with metallic anodes (dendritic growth), interfaces (retardation kinetics of SEI formation) and contact issues (loss of contact over electrochemical cycling) [8].

1.2.1 Electrode Materials

The electrode materials are the major component of a battery. The role-play of the electrode is to maintain integrity and quality over many charge–discharge cycles. The most commercially used cathode materials are layered oxides such as $LiCoO_2$ (LCO), $LiNi_{1-x-y}Co_xMn_yO_2$ (NMC), $LiNi_{1-x-y}Co_xAl_yO_2$ (NCA) & polyanionic compounds such as $LiFePO_4$ (LFP), $LiMn_2O_4$ (LMO), Ni substituted $LiMn_{1.5}Ni_{0.5}O_4$ (LNMO) [10–13] and anode materials such as Li metal, graphite, silicon, $Li_4Ti_5O_{12}$ (LTO), etc., [14] have widely been used in ASSBs.

1.2.2 Electrolyte Materials

The solid electrolyte materials can be inorganic or organic type. The disadvantages of organic liquid electrolytes such as severe capacity losses, decreased cycle life, issues with operation temperatures, safety and reliability could be eliminated with the use of solid inorganic electrolyte materials in ASSBs [15]. The main challenge in developing solid electrolyte material is to achieve the highest ionic conductivity at room temperature (10^{-3} S cm^{-1}) and to onset a conducive solid–solid interface of electrode and electrolyte. The solid electrolytes are majorly classified as crystalline and glassy, namely,

- LISICON type,
- NASICON type,
- Garnet type,
- Perovskite type,
- Glassy type,
- Ceramic type,
- Argyrodite type,
- Solid polymer or polymer composite.

The solid electrolytes with a larger electrochemical window (up to 5 V) are desired for tapping the advantages offered by high-voltage cathode materials as well as of the lithium metal anodes. Argyrodite type of electrolytes with sulphur- and oxide-based compounds such as Li_6PS_{5x} and $Li_7Ge_3PS_{12}$ offer high ionic conductivity but suffer from chemical kinetics with oxide cathodes and hence it is in the arena of tailoring

by several researchers. Solid polymer and polymer filler composites are still under trials to reach the high ionic conductivity with fillers of LISICON or Garnet types of electrolytes. Each type of solid electrolyte is advantageous and discussed in the upcoming sections with their processing techniques.

1.2.3 Different Battery Designs

The requirement of a battery design depends upon various conditions like how much power is needed or what sort of device portability is required. Different design of batteries have been developed based on the applications employed. Most of the conventional LIBs come in a variety of shapes such as coin cell type, cylindrical, prismatic and pouch type.

- **Cylindrical:** Cylindrical lithium batteries possess significantly high specific energy and mechanical stability. The design provides additional safety measures and cycles well, has a long calendar life and inexpensive; however, the package density is less than optimal. It's a popular choice for portable applications.
- **Prismatic:** For stability, prismatic batteries are enclosed in aluminium or steel. It saves space by being jelly-rolled or layered, but it costs more to make than a cylindrical battery. They're commonly seen in electric vehicles and energy storage systems.
- **Pouch:** Lithium battery packed in a compact bag and laminated is a pouch cell. Generally, stacking of individual cells would bring in high internal resistance, however, in a pouch cell, an aggregate of several cells overlaid brings in smaller internal resistance. It is light and inexpensive, but it can be damaged by humidity and extreme temperatures. By preventing delamination, adding a light stack pressure extends the life of the product [9].

The different designs of batteries like all-solid-state batteries, thin-film batteries, thin-film paper batteries, flexible batteries, silicon-based ASSBs, 3D thin-film batteries, single-phase ASSBs and lithium metal batteries along with their salient features are discussed in the below section.

1.2.3.1 All-Solid-State Batteries

The dense lithium lanthanum titanate prepared from spark plasma sintering with lithium manganate cathode and Li metal as all-solid-state battery in the early 2000s, where one of the authors had contributed, yielded 4.3 V at 60 °C [16].

The fabrication of all-solid-state battery using a ceramic type electrolyte, Li|$Li_5La_3Ta_2O_{12}$ (LLTa)| $LiCoO_2$, was studied. This ceramic electrolyte LLTa, due to its high Li-ion conductivity and good stability when assembled as full cell, is a prospective candidate for all-solid-state battery. After one complete year of long-term storage, the fabricated cell was found to be operated successfully without any

deviation of the redox peaks even upon cycling. But the specific capacity obtained was only 4% of the theoretical capacity value and reported that this may be due to low utility of cathode and less wettability of solid electrolyte on $LiCoO_2$ cathode [17].

To overcome these issues, the same group of researchers has worked on three-dimensional battery modelling by introducing a three-dimensionally ordered macroporous (3DOM) $Li_{1.5}Al_{0.5}Ti_{1.5}(PO_4)_3$ (LATP) composite electrodes. This is a novel method and provides larger surface area and declines the internal resistance of the cell. The discharge capacity of the full cell containing LATP composite electrodes with a polymer electrolyte shows a discharge capacity of 480 $\mu Ahcm^{-2}$ and found that the electrochemical performance could be improved by using composite electrodes with higher filling ratios [18].

1.2.3.2 Thin-Film Batteries

All-solid-state battery technology includes thin-film LIBs. Thin-film batteries are lighter in weight, have high energy density and are suitable for wearable devices. Thin-film micro-batteries typically have a Li metal as anode, a polymer type or lithium phosphorus oxynitride $Li_{3+x}PO_{4-x}N_x$, (LiPON) electrolyte and lithium-based oxides as cathode. LiPON is the most remarkable Solid Electrolyte (SE) developed by Oak Ridge National Laboratory that possesses considerable stability in air compared to other oxide and sulphide-type electrolytes. A thin-film solid-state battery is fabricated using TiO_2 anode, lithium—nickel–manganese–cobaltite (LNMC) cathode and LiPON electrolyte and the assembled cell shows a capacity of 52 $\mu Ah\ cm^{-2}\ \mu m^{-1}$ (a special unit for thin film batteries) with a capacity retention of 90% over 400 cycles [19].

1.2.3.3 Thin-Film Paper Batteries

Thin-film Li-ion paper batteries have been fabricated using a simple lamination process on a single sheet of paper. This type of flexible battery is rechargeable and exhibits a higher energy density of 108 mWh g^{-1}. As the total mass of the device is too small with miniaturization these could be employed in RFID tags, wearable devices, functional packaging and new disposable biomedical applications [20].

1.2.3.4 Silicon-Based Thin-Film Batteries

Recently, silicon-based thin-film Li-ion batteries are developed due to the possibility of the formation of intermediate and reversible alloy $Li_{15}Si_4$ with a theoretical capacity of 3579 mAh g^{-1}. However, the volume changes up to 300% during lithiation/delithiation process remain a severe drawback with silicon as anode material [21, 22]. Silicon-based anodes are a good choice for ASSBs [21]. But severe volume

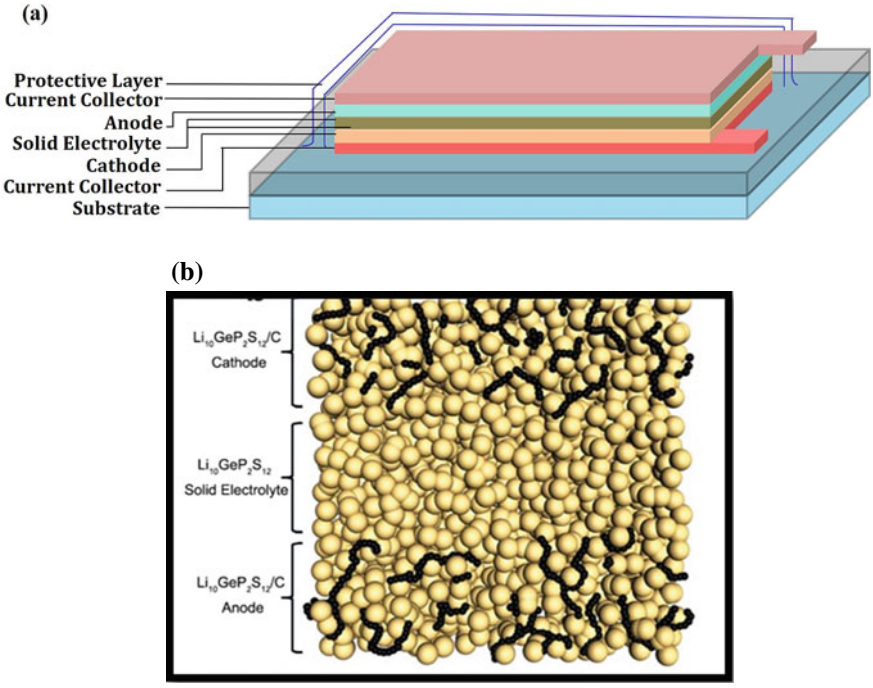

Fig. 1.2 **a** Schematic diagram of a thin-film battery. Copyright Permission from [22] ACS Nano., 11(5), 4731–4744, 2017. **b** Schematic diagram of ASSBs assembled with single-material LGPS Copyright permission from [23] Chem. Commun., 54, 3178–3181, 2018

changes during the cycling process lead to degradation. The introduction of carbon thin-film layer (both on surface and inter layer) upon Si electrode was demonstrated which could increase the electrochemical performance and the mechanical stability (Fig. 1.2a) [22].

The column structure of silicon provides a 1D breathing mechanism like that of lithium which tends to preserve the interface with the electrolyte. The column silicon (col-Si) anode was prepared by Physical Vapour Deposition (PVD) technique and fabricated as a full cell with argyrodite type electrolyte Li_6PS_5Cl and Ni-rich NMC cathode ($LiNi_{0.9}Co_{0.05}Mn_{0.05}O_2$,) resulted in an outstanding performance with a capacity retention of 82% over 100 cycles and reversible cycling without short-circuiting for more than 350 cycles. This report shows an excellent performance with a new kind of column silicon anode with a pouch-type assembly [24]. Slurry mixed sheet type Silicon-Polyacrylonitrile (Si-PAN) anodes along with argyrodite-type electrolyte and NMC cathode were assembled in a pellet-type configuration and reported towards the commercialization of ASSBs [25].

1.2.3.5 3D Thin-Film Batteries

Three-dimensional thin-film batteries has been experimentally realized by Alexander Pearse et al., in 2018 [26]. The 3D batteries show both power and energy density benefits where a pre-lithiated vanadium pentoxide (V_2O_5) cathode, a very thin layer of Li_2PO_2N solid electrolyte (40–100 nm) and SnN_x anode have been employed. The assembling of this battery was done using Atomic Layer Deposition (ALD) technique [26].

Nam et al. [27] explained a process that could improve the ionic conductivity of the electrolyte and demonstrated that the premixing of solid electrolyte and active material would improve the electrochemical performance. The authors have demonstrated the intrusion and the hindrance caused by the polymer binder in the performance and contact. In addition, they have also exploited and reported the effects of both (i) the coating of $LiNbO_3$ on NMC cathode through wet chemical method and (ii) dry mixing and achieved better performance with a scalable process. Lithium nickel cobalt manganese oxide ($LiNi_{0.6}Co_{0.2}Mn_{0.2}O_2$) cathode and graphite anode are dry mixed without any addition of binder and slurry mixed with the addition of polymeric binder and assembled as a full system using an argyrodite-type solid electrolyte (Li_6PS_5Cl). The slurry mixed electrodes showed good electrochemical performance and this was taken for full cell fabrication, viz. pelletized cell and an 80 $\times$ 60 cm^2 (NMC6221 graphite type) pouch-type cell. The pouch-type cell showed a high energy density of 184 Wh kg^{-1} and analysed for safety tests by charging the cell to 4.3 V at 0.025 C which was then cut with scissors and no noticeable changes were observed and hence justified the mechanical robustness of solid electrolyte [27].

1.2.3.6 Single-Phase ASSBs

In 2015, Han et al. developed a single-material battery made up of $Li_{10}GeP_2S_{12}$ (LGPS). As the area of contact, as in liquid electrolyte, could not be achieved, in both transport aspects and infiltrative aspects, with solid electrolyte, high resistance interface and lack of sufficient interfacial contact limit the transport of lithium thus reducing the active sites. So as to address the interfacial problem, a novel single-material ASSLIB was developed with LGPS. It acts as a Li_2S cathode and GeS_2 anode when LGPS is coupled with carbon that creates active centres of Li–S and Ge–S that are reversible, which in turn reduces the interfacial issues [23]. From the insight of the literature reported in 2012, $LiTi_2(PO_4)_3$ (LTP) solid electrolyte, due to the presence of the Ti^{4+}/Ti^{3+} redox pair, more suits to be employed as both electrolyte and an anode [28].

Therefore, in the year 2018, Inoishi et al. thought that if this kind of material could also act as cathode, there is a chance of developing a single-phase ASSBs and found that Cr-doped LTP can satisfy the expectation. The configuration of the assembled single-phase battery was Pt/$Li_{1.5}Cr_{0.5}Ti_{1.5}(PO_4)_3$/Pt. Hence, this NASICON-type $Li_{1.5}Cr_{0.5}Ti_{1.5}(PO_4)_3$ resulted in superior conductivity and low-interfacial resistance which was beneficial to overcome the interface-related issues [29]. In 2019, Chen

et al. designed an all-solid-state battery in which the total packaging and components were found to be stretchable. Different stretchable electrodes were reported in literatures but processing them into full cells is described rarely. Hence, assembling a stretchable battery is reported by this team of researchers. The choice of current collector must remain stretchable so as to confirm the elasticity of the cell hence a stretchable carbon composite conductive layer is chosen where Ag nanoflakes were deposited. The stretchable electrodes were fabricated by combining the active materials onto the elastic current collector. This study showed that, on stretching the battery to 50%, a reversible capacity of 28 mAh g^{-1} and an average energy density of 20 Wh kg^{-1} were obtained after 50 cycles [29].

Some of the remarkable literatures with the full cell configuration and electrochemical properties are shown in the Table 1.1.

1.2.3.7 All-Solid-State Lithium Metal Batteries

All-solid-state lithium metal batteries are promising candidates since lithium, with its ultrahigh capacity (3860 mAh g^{-1}), remains a holy grail for all battery technology and a metal possessing the lowest reduction potential [30]. The Li dendrite growth is prevented by alternate methods of either encapsulating with organic or inorganic compounds. Some of the recently reported remarkable literatures on lithium metal batteries are shown in Table 1.2.

1.3 Processing Techniques for ASSBs

The processing of all-solid-state batteries depends on the nature of materials and application to be employed for. There are many techniques which could be employed based on the lab scale or the industrial scale. The processing of full cell using different techniques are discussed below.

1.3.1 Wet Coating Process

The wet coating process is a convenient method for large-scale coatings in industries. In this technique, the material to be coated on a substrate is dispersed or dissolved in a liquid solvent. The coated wet film is subjected to drying and post-processing, namely, (i) hot-pressing—that can achieve compaction thus increasing the density or (ii) calendaring or laminating—is also compression of electrodes after drying that reduces porosity thus bringing better contact between the particles, in turn, bringing betterment in energy and power density. Generally, organic solvents used in the preparation of electrodes possess severe environmental and safety concerns which is the necessary point of developing an aqueous process [34]. Due to the fast drying

Table 1.1 Design of all-solid-state lithium-ion batteries and their electrochemical performance

S.no.	Anode	Electrolyte	Cathode	Electrochemical performance	Method of assembling	Refs.
1	Li-metal	$Li_5La_3Ta_2O_{12}$ (LLTa)	$LiCoO_2$	Specific capacity 3862 mAh g^{-1}	Pellet	[18]
2	TiO_2	Amorphous (LiPON)	LNMC ($LiNi_{1/3}Mn_{1/3}CoO_2$)	Cell capacity of 52 μAh cm^{-2} μm^{-1} with 90% capacity retention after 400 cycles	Thin-film	[19]
3	Columnar silicon (Col-Si)	Argyrodite-type Li_6PS_5Cl	NCM ($LiNi_{0.9}Co_{0.05}Mn_{0.05}O_2$)	Specific capacity of 210 mAh g^{-1} and stable cycling for more than 100 cycles	Pouch	[24]
4	Si-PAN	Argyrodite	Nickel-rich NMC 811 composite	Specific capacity of 1500 mAh cm^{-3} at current density <0.2 mA cm^{-2} for 100 cycles at 1C rate	Coin cell	[25]
5	SnN_x	Li_2PO_2N	LiV_2O_5	Energy density and power density of 3.9 mWh/cm^2 and 386 mW/cm^2 for 400 cycles at 5 μA/cm^2	Coin cell	[26]
6	$LiNi_{0.6}CO_{0.2}Mn_{0.2}O_2$/graphite (NCM622)	Gel polymer electrolyte	$LiNiCO_2$	Specific capacity of 372 mAh g^{-1} for 200 cycles at 1C rate and energy density 184 Wh kg^{-1}	Pouch type	[27]

Table 1.2 Design of all-solid-state lithium metal batteries and their electrochemical performance

S.no.	Anode	Electrolyte	Cathode	Electrochemical performance	Method of assembling	Refs.
1	Silver carbon nanocomposite layer (AgC)@ no excess Li metal	Argyrodite-type Li_6PS_5Cl	$LiNi_{0.90}Co_{0.05}Mn_{0.05}O_2$ (NMC)	Energy density 942 Wh L^{-1} and discharge capacity of 5,870 mAh g^{-1} with superior cycle life >1000 times	67 × 112 mm bi-cell-type pouch cell	[31]
2	LiPFG@Li	Argyrodite-type Li_6PS_5Cl	$LiZrO_3$ @ $LiCoO_2$	High reversible capacity of 125.7 mAh g^{-1} at 0.1C and lifetime of over 80 cycles	Coin cell	[32]
3	Li metal	PVA/PAN/LiTFSI/ LATP/ SN	$LiFePO_4$	Discharge capacity of 119.4 mAh g^{-1} at 0.5 C, exhibiting a capacity retention of 90.5% after 100 cycles at room temperature	Pouch cell	[33]

nature that results in fractal formation and discontinuity with aqueous slurries, the demand for organic content in the slurry becomes essential. Aqueous-based electrode preparation methods are hence not suitable [35]. Several techniques such as doctor blade, slot die coating, dip coating, etc. One of the most convenient methods for the formation of composite electrode and solid electrolyte is wet coating technique [36].

Doctor blade technique otherwise known as tape casting or knife coating is the most commonly used technique in batteries [37] and achieves a coating thicknesses <50 μm. Several large-scale processing like (i) comma bar—the wet coating slurry is directly applied to the current collector or conveyed using an applicator roll to the current collector, (ii) reverse comma roll—The coating is achieved with one applicator roll is driven by a support roll from where the metering roll gets the slurry coated where the current collecter is placed (iii) Knife over roll coating—where a conveyer is placed very close to the knife and the current collector is placed upon. The slurry is dispensed on the current collector and a knife meters the slurry to achieve the coating, (iv) Meyer rod coating- a Meyer bar with uniform pitched groove rolls and picks up slurry and metres where a subsequent roller rolls the coated current collector. The above-said methods being the mechanical methods few volumetric methods are also advantageous on a large scale.

Gravure method—where the slurry is delivered to the rolling current collector using a pattern engraved transfer to the applicator roll. The smoothness of coating depends on the closeness of the pitch in the pattern. The suitability of method depends on the viscosity, shear level, coating thickness, mass loading and uniformity achieved. Among all, the doctor blade method is more commonly used. Tape casting technique is used for the process of polymer electrolytes where a polymer and conducting salt are dissolved in an appropriate solvent and casted on a non-porous substrate. The dried membrane is now the electrolyte membrane obtained which can be removed after drying [38–42]. Hot pressing of electrode and electrolyte layers is done after the drying process. The control over the thickness of the membrane and handling is made easier when fabricated using this technique [43].

Spin coating technique (Fig. 1.3b) can be used for the preparation of thin-films of solid electrolytes [44–46]. The scalability of this method is questionable on the fact of large-scale coverage, homogeneity of the film and uniformity of the formed films. Usually, a small amount of material is placed on the substrate which is subjected to different spinning speeds and times and then dried and further rotated to form multi-layered structures. Dip-coating technique (Fig. 1.3c) is widely used for the coating of separators in Lithium battery processing [47, 48]. The typical dip-coated films are in the nanometer range which can be used for surface modifications of pre-formed electrode and electrolyte layers. It is remote to employ this technique for the preparation of electrodes and solid-state electrolytes [49–51].

Slot-die coating is another interesting method for large-scale production of wet electrode processing [57]. Slot-die method has a slotted die in which the slurry is transferred to the roller or conveyor mounted with the current collector. The internal cavity and the orifice of the slot die determines the coating quality. Faster the substrate mobility thinner is the metered coat. The metred coat also depends on the size of the orifice and the viscosity of the slurry. Several layers of overlay can also be made to

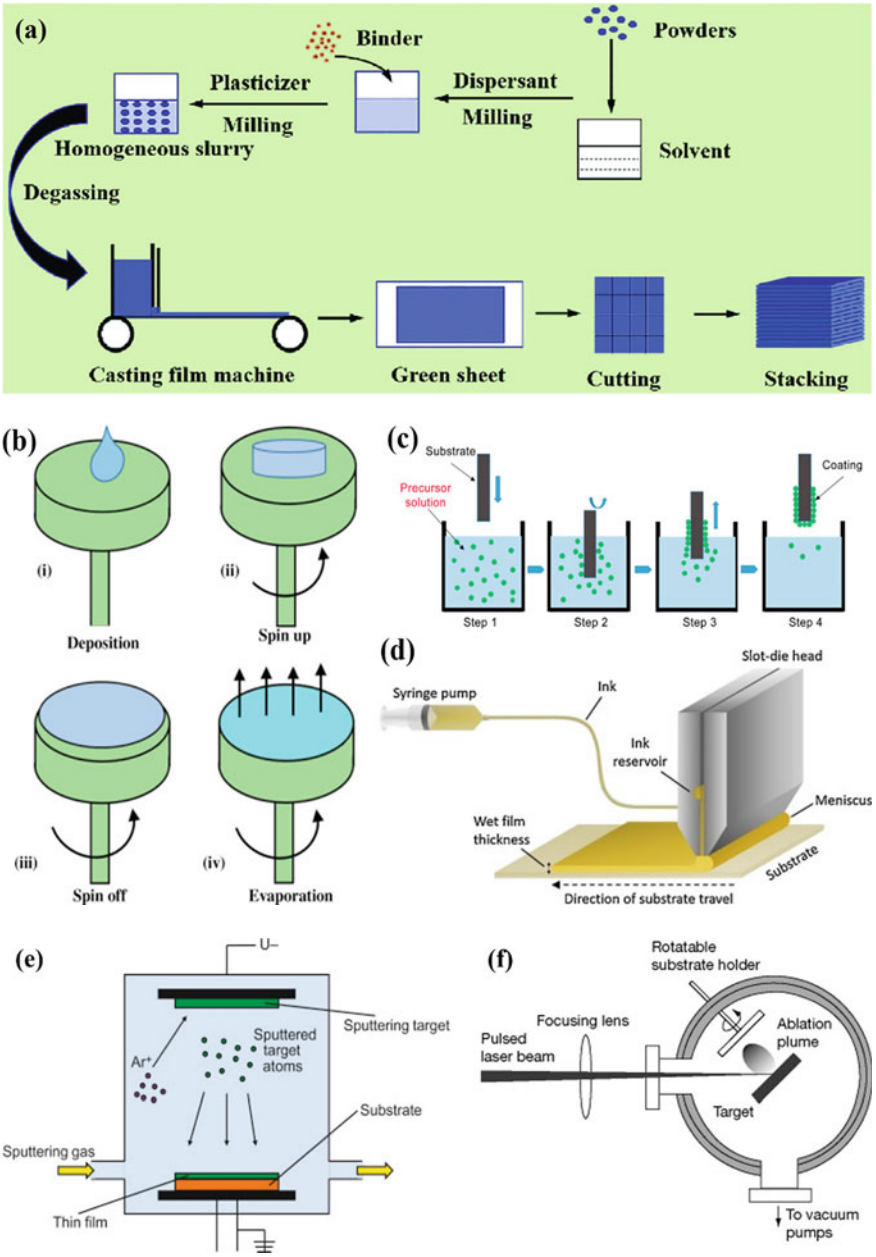

Fig. 1.3 **a** Tape casting technique [42]. Stages of (**b**) Spin coating process Copyright permission from [52] Elsevier, 4, 45–98, 2019 **c** dip-coating process Copyright permission [53] from, Elsevier, 4, 271–295, 2016 and **d** slot-die coating process. Copyright permission from [54] Materials Today Communications, Elsevier, 2020. **e** Schematic diagram of Physical Vapour Deposition process (PVD) Copyright permission from [55] Severe Plastic Deformation Elsevier, pp. 1–17, 2018 **f** Pulsed Laser deposition (PLD) [56]

form multi-layered films, especially when the interfacial layers in ASSBs are made to offer a transient interface for the reduction of internal resistance. Figure 1.3d shows the loading of slurry using a syringe pump, marked as ink, which is fed to the slot die heater and consequently the film is formed as a wet film. It is to be noted that the meniscus formation is the hurdle as the film would lose uniformity hence an over drag is always necessary with this type of coating to avoid inhomogeneity in the film.

Mostly inorganic or sulphide-based solid electrolytes are coated using wet coating techniques. Pellet-type cells are the most favourable design when solid electrolytes are used with a composite type of cathodes where cold sintering and hot sintering will be annexed to the processing. Sheet-type or pouch-type cells are fabricated by mixing the solid electrolyte powder with the polymer binder by wet-coating process and pressing [58]. A very recent publication explored the utility of electrospinning for polyimide porous separator on argyrodite type of solid electrolyte [59]. The wet-coating techniques are widely suitable for lithium polymer cells and sulphide based cells. Utilization of organic solvents is inevitable in any of the wet coating techniques and comes with a limitation posed due to the side reactions between residual solvent and metallic lithium and the inhomogeneity in the membrane caused during the drying process. And also pore formation during solvent evaporation makes room for the unwanted reactions to happen between solid electrolytes and electrodes in all-solid-state batteries [60].

1.3.2 Extrusion Process Devoid of Solvent

The extrusion process devoid of solvent is more cost-effective than the wet coating technique since there is no use of toxic organic volatile solvents in the process of SEs [61, 62]. In developing lithium battery electrolytes and electrodes, a significant progress is made towards cost-effectiveness and environment compatibility by extrusion process without solvent. Many porous/non-porous electrodes and polymer electrolytes are prepared by this method.

The extrusion process consists of three main steps, namely:

(i) The blending of materials in molten state for preparing viscous formulations,
(ii) The film forming process by die casting using a flat film die,
(iii) Rolling the extruded film between two chilled rollers causing a quenching effect. Several parameters, namely, temperature and shear parameters related to degradation and physical property change are expected. Due to the heavy pressure subjected on rolling the molten material (rheological properties), glass transition temperature or glassy formation due to the quenching effect where the rate of cooling influences has a major role. One good advantage of this method is that it is devoid of post-processing; however, thickness and homogeneity-related issues need to be resolved, especially in polymer electrolytes. Except for sulphide-based electrolytes all the other inorganic electrolytes can be extruded directly and a post-annealing step at high temperature is needed [63]. This

method of melt extrusion is found to be the best method for polymer electrolyte. In recent days, not only polymer electrolytes but also electrodes are prepared by extrusion method as it is more suitable for large-scale production [64]. An additional advantage of this method is that both electrode and electrolyte slurries can be co-extruded using two separate flow channels with a single-slot die thus reducing the production cost as well as would improve interfacial contact [65].

Looking in chronology, the earlier one to report the co-extruded lithium polymer battery was Baudry et al. [66]. A variety of composite polymer electrolytes prepared by the melt method were studied by Gonzales et al. [64, 67, 68]. Melt extrusion and co-extrusion are found more suitable for the ceramic-rich composite electrolytes. Ta-doped LLZO-based SSBs are prepared by melt extrusion method with post sintering and lamination processes by Herle and Gordon [69]. The ease of scaling up for large-scale production and environmentally benign nature due to the absence of toxic solvents mark the melt extrusion process a more preferable one in the mass production of solid-state batteries with polymer components.

1.3.3 Printing

The present conventional batteries available in the market are standardized ones with the fixed geometries and shapes either by stacking if they are planar cell or by winding if it is a cylindrical cell. The films are either punched to the standardized dimension followed by stacking or winding and post-filling the liquid electrolyte [70]. The 2D and 3D architectures are designed in order to improve the specific capacity and flexibility of batteries. The electrochemical active area and sites are increased in the 2D and 3D batteries which could increase the overall performance of the battery.

1.3.3.1 2D Printing Techniques

The 2D printing technologies are classified into contact and non-contact techniques. The contact techniques are flexographic printing [71], screen/stencil printing [72], imprint lithography technique [73] and non-contact techniques such as spray deposition [74]. The contact techniques such as screen printing are classical and used commonly due to their wide scalability and simplicity [61]. In this technique, a patterned mask or a stencil is placed on the substrate and the slurry is passed through that to the substrate. The excess slurry is not allowed to infuse and hence wiped out from the top. Flexographic printing—2D-printing technique can also be employed since it is also a roll-to-roll model yielding a continuous film. The printing process of solid electrolyte is in its infant stage but getting more popularity due to its simplicity and scalability. Usage of stencil with UV curable polymer electrolytes and electrodes in the required geometries or customized shapes offers flexibility in the preparation of

batteries based on the demands posed by the novel gadgets and miniaturized modern appliances [75, 76].

1.3.3.2 3D Printing Techniques

The process which allows fabricating parts of 3D materials is otherwise known to be additive manufacturing (AM). It paves a way to obtain complex geometries than 2D printing. Stereolithography—photo-polymerizable precursor will be cured through an appropriate light source; material jetting technique—ejection of material in the form of ink or aerosol through a nozzle; and material extrusion technique—ejection of material through an orifice which is directly transferred to the target [77] and by fused deposition modelling [78, 81]. The 3D printing is found to be the most suitable technology for processing solid polymer electrolytes and is considered to be used for various applications such as the production of micro-batteries, cables- or fiber-type batteries, for wearable applications (state).

1.3.4 Pressing

Three aspects can be improved while employing the pressing technique for the fabrication of solid-state batteries. The densification or compaction of the solid electrolyte firstly improves the ionic conduction, secondly brings in better chemical stability between the ionic conducting component and the electronic conducting component and thirdly, attains good contact or wettability between the solid electrolyte and the electrodes. Materials are taken in powder form and pressed using a uniaxial shaft or plunger depending on the size of the pellet and pressed iso-statically or pseudo-iso-statically to form a pellet. Generally, pressed pellets to perform well when the particle size of the components is smaller (say better with nanoscale particles than microscale particles). Pressing can be done either at room temperature or at low temperature thus the compaction brought is only by pressure. When high temperature is applied, say sintering with pressure, thermal energy plays a major role. A suitable example for this is the spark plasma sintering process where there is a pressure applied and simultaneously thermal energy is utilized to bring compaction and hence would bring a drastic reduction in the grain boundary thus improving the ionic conductivity in the solid electrolyte, especially ceramic electrolytes.

1.3.4.1 Low-Temperature Pressing

First, a report on low-temperature pressing by Hans et al. in 1966 on cold pressing made a breakthrough in metallurgy [80]. Further improvements on pressing modes and temperature-controlling systems have been brought in the past. Present-day batteries essentially employ calendaring which is a low-temperature pressing process.

The tape-casted membrane is pressed with heated rollers that smoothen and compress the membrane and improves contact and mechanical stability [81] holds good for an extruded film also [82]. The temperature limit of pressing depends on the nature of material used say, for polymers, it has to be below 100 °C; otherwise, denaturization of polymer occurs [83], whereas, for ceramic material, high temperature is necessary to bring in changes in the material. On contrary, LISICON-based amorphous oxide has been cold pressed using a heavy load of 800 MPa with a subsequent sintering process for solid-state battery fabrication [84]. Few researchers have used hot pressing for assemblies with polymer membranes as well.

1.3.4.2 High-Temperature Sintering

Conventionally, sintering ceramics happens at very high temperatures typically above 1000 °C. The sintering temperatures are chosen based on the factors such as the nature of material, particle size, sintering atmosphere, etc. [85]. High temperatures are well handled on laboratory scale in battery research however when the pilot production is targeted many of the processes find a hindrance in handling such high temperatures and the running costs would be taken high. There are different types of high-temperature sintering listed as follows:

- Hot pressing [86, 88],
- Hot isostatic pressing [88],
- Field-assisted sintering [89],
- Flash sintering [90],
- Microwave sintering [91, 92],
- Spark plasma sintering [84, 93–96] and
- High-pressure field-assisted sintering [95].

Majority of material on high-temperature sintering are of high density and improved mechanical properties. The hamper in this process is the choice of material and thermal stability accounts high for employing this method.

1.3.4.3 Cold Sintering

Cold sintering process is achieving compaction at temperatures less than 400 °C through transient transport of a fluid, mostly liquid, along with applying a uni-axial pressure of high magnitude in GPa. In this method, the densification achieved is quite similar to the thermal process in addition, the activation energies obtained will be lower than the thermal sintered material due to the grain boundary creeping or crystal nucleation at grain boundaries. But, it is a multistep process where particle surface dissolution, evaporation of solvent are involved that makes this method less captive for commercial production. Further improvements are still being made by

several groups with diversified material that demands high-temperature sintering. In this process, favourable results are obtained either due to the grain growth through creeping or crystal nucleation at grain boundary leading to grain fusion or due to the prevention of glassy interface generally formed due to the quenching effects from high temperature in the conventional thermal method [96, 97].

1.3.5 Thin-Film Deposition

Deposition techniques are quite frequently used in forming micro-batteries or in forming protective layer(s) towards stabilizing chemically active interfaces. It has also been used for the (i) deposition of Li thin-film anodes [9], (ii) ceramic films—inorganic electrolytes thin-film [99–101] and (iii) for creating protective coatings when interfaces are unstable [102]. To state a few, the growth of amorphous LiPON [103] or coated interface for LLZO or LLTO with oxide electrodes are good references [104, 105]. Under vapour deposition, electrodes can also be formed using physical vapour deposition (PVD)—Evaporation, Sputtering & Pulsed layer deposition (PLD) and Chemical vapour deposition (CVD) or methods [55]. Sequential depositions of solid-state electrodes and cathodes bring down the interfacial issues of wettability and the choice of materials based on vapour pressure is the key issue when performing this method.

1.3.5.1 Physical Vapour Deposition

PVD is a process in which material is deposited from the gas phase. Its main benefit is the ability to create dense solid layers with variable thickness, composition, crystallinity and crystal orientation (Fig. 1.3e). PVD has a number of distinct advantages, including the ability to densify materials at substantially lower processing temperatures than traditional heat treatment due to the increased energy of the plasma.

- **Evaporation**

Direct evaporation of a material (a metal) placed in a thermal source driven to the target when the heat is raised to the evaporation point of the metal, the coating is achieved. Thermal evaporation can be made through the resistive heating of elements or by e-beam evaporation using an intense electron gun to heat the substance. Bates et al. demonstrated deposition of metallic Li film having Li anode by the process of evaporation [98] and secondary coating of In, Al, etc., on Li foils their performance have been reported. Improved wetting properties of Li on certain ceramic electrolytes by forming Lithium alloys of reversible nature have also been demonstrated [106, 107].

- **Sputtering**

The principle of sputtering is to bombard high energetic particles of a plasma or gas on a dense target material and ejecting out microscopic particles that are collected on a substrate driven by a high voltage across the electrodes to form a film. In ASSBs, DC sputtering is chosen as an alternative to evaporation due to better adhesion and higher packing density. Generally, deposited elements are Li, Mg [108] and Au [109]. While coating protective layers on ceramic materials RF sputtering or reactive DC sputtering to prevent charging or when additional elements like alloy formation are required. For example, Li on Al_2O_3 anodes [110] or Li on SnO_2 [111], or the deposition of electrolytes such as LiPON [112] or LLZO [113].

- **Pulsed Laser Deposition (PLD)**

In PLD, a high-energy pulsed laser ablates a dense pellet of the required coating material mounted in the target (Fig. 1.3f). The ablation creates plasma of ionized particles of the ablated material and is directed to the substrate to form the film. PLD acquired more popularity as the process is highly flexible as the energy source (laser) is outside the coating chamber, control of the deposition process is possible and any material can be ablated, preservation of stoichiometry. Most of the ceramic materials that are not viable for coating with evaporation method due to vapour pressure difference in the compound can be ablated to film using this method. Especially, for most of the state-of-the-art ceramics oxide electrolytes PLD offers good performance (LiPON, LLTO, LLZO, etc.) [100]. Still, when depositing Li-containing films, more caution is required, since recent investigations have revealed significant Li loss on coating. Loss of lithium is a common issue with thermal processes where the excess lithium will be added intentionally to arrive at the required stoichiometry. Any process that develops more than 300 °C is likely to have lithium loss since lithium can contaminate a vacuum at this temperature. Several techniques have been demonstrated to be effective in compensating the lithium and so the same with the ablated target [105] or the pre-coated lithium thin-film on the substrate by means of multilayer deposition [104]. Today, significant attempts are being made to scale up the PLD process to an industrial scale, primarily to arrive at a homogeneous large area deposition. So far, equipment have also been developed to increase the area of deposition up to 150 mm diameters with an allowance of integration to batch manufacturing. However, a commercially viable scaling is a desirable one till now.

1.3.5.2 Chemical Vapour Deposition (CVD)

The Chemical Vapor Deposition (CVD) is a process of growing desired material which is a byproduct of two or more reactants reacting chemically. The Atomic Layer Deposition (ALD) is one of the CVD processes that can also be used for depositing film protective layers while assembling SSBs [114]. In ALD, a substrate will be exposed to precursors alternatively to make multilayers of atomic dimensions to form films. This process can bring out ultra-thin layers of nanoscale. The temperature, time

of exposure, purging time of precursor and the carrier gas flow rate determines the quality of films. Several cathode materials have been deposited using this method that includes cathodes ($LiFePO_4$ [115], $LiCoO_2$ [116]), anodes ($Li_4Ti_5O_{12}$) [117] and ceramic electrolytes (LiPON [118]), LLZO [119].

1.4 Interfacial Challenges for Full Cell Development

Unlike existing LIBs, which rely on liquid electrolytes to wet the cathode and anode to facilitate Li-ion transmission, SSBs require precise wettability between the various components and electrolytes. A good interface will be having utmost compactness between the components offering low resistance; will have long-term stability on cycling and no intermediate irreversible compounds to be formed on cycling.

It would be a wise option to study the compatibility of two components of the battery before assembling a solid-state battery. The predictive analysis of internal resistance by analysing the mixture of two components would save different trials of battery designs. The major interface of the anodic side is Li metal to solid electrolyte where dendrite formation and irreversible alloy formations are the major issues to be addressed. If the SE is a composite material, the segregation of composite during intercalation and de-intercalation process leaves irreversible aggregation of elements at the solid electrolyte side in the cathodic side [120] at the cathodic interface. When conductive additives and binders are used, several interfaces coexist. Finally, the interface between the current collector and the cathode (Fig. 1.4a) is the key interface where the choices of current collectors need to be critically made. Redesigning and adapting the battery production chain to solid-state batteries is a critical task, in the view of multiple interfaces coexisting that includes complexity and their physical properties.

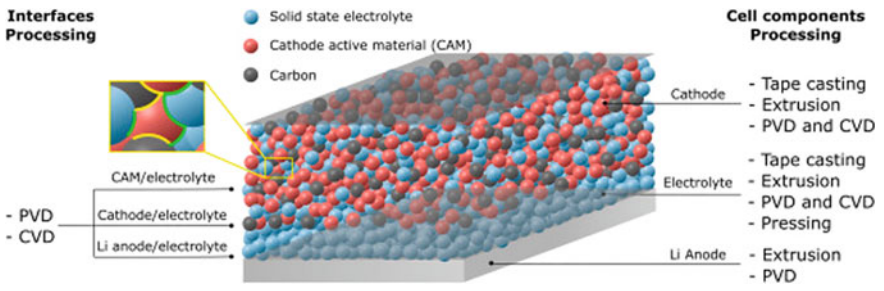

Fig. 1.4 **a** ASSBs full cell development showing both interface and cell components processing Copyright permission from [121] J. Power Sour., 502, 2021, Art.No. 229919

1.4.1 Interfaces at Composite Solid Cathodes

Many interfaces are created as a result of cell integration, both at intercomponent (electrode/electrolyte, CAM/electrolyte, current collector/electrolyte) and at intra-component (composite, conductive additives and adhesive additives). Interfacial issues account for a large portion of the challenges encountered during the implementation of an SSB. Charge accumulation at the interface and mass transfer resistance due to poor contact in the electrolyte to cathode interface is a major challenge. Increasing the wettability or compaction or addition of mixed layers of SE material and cathode will improve the performance of the assembled SSB.

1.4.2 Interfaces at Li Metal and Electrolyte in Solid-State Batteries

As stated already, Li metal is the commonly used anode material forming the interface with solid electrolyte. Volume change due to lithiation and de-lithiation over cycling, formation of lithium dendrites that leads to short circuit which is the key factor for thermal runaway and degradation of anode on cycling due to secondary phase formation is the key burning issues addressed by battery researchers [122].

1.4.3 Interfaces at Current Collector

Current collectors are the messengers between the battery components and the payload. Mostly the current collectors offer mechanical support on which the composite cathode is casted. The interface caused is not given much importance however this also plays a vital role in bringing the internal resistance of the full cell down since it can bring chemical and electrochemical instability to the fabricated SSB [123]. Choice of current collector is very vital and in common, aluminium is the preferred current collector in the lithium transition metal oxide (Popular NMC) cathodic side and also for the cathodes of 5 V (LFP) versus Li/Li^+ [124]. Though the native Al_2O_3 passivating layer grown on the Al surface is used as protection for the current collector as corrosive resistant, many of the salts do not go well with these layers inviting issues of additional type to the assembled SSBs.

40. Du, M., Liao, K., Lu, Q., Shao, Z.: Recent advances in the interface engineering of solid-state Li-ion batteries with artificial buffer layers: challenges, materials, construction, and characterization. Energy Environ. Sci. **12**(6), 1780–1804 (2019)
41. Wang, D., Sun, Q., Luo, J., Liang, J., Sun, Y., Li, R., Adair, K., Zhang, L., Yang, R., Lu, S., Huang, H.: Mitigating the interfacial degradation in cathodes for high-performance oxide-based solid-state lithium batteries. ACS Appl. Mater. Interfaces **11**(5), 4954–4961 (2019)
42. Sun, C., Liu, J., Gong, Y., Wilkinson, D.P., Zhang, J.: Recent advances in all-solid-state rechargeable lithium batteries. Nano Energy **33**, 363–386 (2017)
43. Manthiram, A., Yu, X., Wang, S.: Lithium battery chemistries enabled by solid-state electrolytes. Nat. Rev. Mater. **2**(4), 1–16 (2017)
44. Krauskopf, T., Dippel, R., Hartmann, H., Peppler, K., Mogwitz, B., Richter, F.H., Zeier, W.G., Janek, J.: Lithium-metal growth kinetics on LLZO garnet-type solid electrolytes. Joule **3**(8), 2030–2049 (2019)
45. Grazioli, D., Zadin, V., Brandell, D., Simone, A.: Electrochemical-mechanical modeling of solid polymer electrolytes: stress development and non-uniform electric current density in trench geometry microbatteries. Electrochim. Acta **296**, 1142–1162 (2019)
46. Wang, P., Qu, W., Song, W.L., Chen, H., Chen, R., Fang, D.: Electro-chemo-mechanical issues at the interfaces in solid-state lithium metal batteries. Adv. Func. Mater. **29**(27), 1900950 (2019)
47. Bucci, G., Swamy, T., Chiang, Y.M., Carter, W.C.: Modeling of internal mechanical failure of all-solid-state batteries during electrochemical cycling, and implications for battery design. J. Mater. Chem. A **5**(36), 19422–19430 (2017)
48. Wang, M., Sakamoto, J.: Correlating the interface resistance and surface adhesion of the Li metal-solid electrolyte interface. J. Power Sources **377**, 7–11 (2018)
49. Han, F., Zhu, Y., He, X., Mo, Y., Wang, C.: Electrochemical stability of $Li_{10}GeP_2S_{12}$ and $Li_7La_3Zr_2O_{12}$ solid electrolytes. Adv. Energy Mater. **6**(8), 1501590 (2016)
50. Koerver, R., Zhang, W., de Biasi, L., Schweidler, S., Kondrakov, A.O., Kolling, S., Brezesinski, T., Hartmann, P., Zeier, W.G., Janek, J.: Chemo-mechanical expansion of lithium electrode materials—on the route to mechanically optimized all-solid-state batteries. Energy Environ. Sci. **11**(8), 2142–2158 (2018)
51. Ito, S., Fujiki, S., Yamada, T., Aihara, Y., Park, Y., Kim, T.Y., Baek, S.W., Lee, J.M., Doo, S., Machida, N.: A rocking chair type all-solid-state lithium-ion battery adopting Li_2O–ZrO_2 coated $LiNi_{0.8}Co_{0.15}Al_{0.05}O_2$ and a sulfide-based electrolyte. J. Power Sources **248**, 943–950 (2014)
52. Peled, E., Yamin, H.: Solid electrolyte interphase (SEI) electrodes. Part 1. The kinetics of lithium in $LiAlCl_4$–$SOCl_2$. Isr. J. Chem. **18**(1–2), 131–135 (1979)
53. Kong, S.T., Deiseroth, H.J., Maier, J., Nickel, V., Weichert, K., Reiner, C.: Li_6PO_5Br and Li_6PO_5Cl: the first lithium-oxide-argyrodites. Z. Anorg. Allg. Chem. **636**(11), 1920–1924 (2010)
54. Woo, J.H., Trevey, J.E., Cavanagh, A.S., Choi, Y.S., Kim, S.C., George, S.M., Oh, K.H., Lee, S.H.: Nanoscale interface modification of $LiCoO_2$ by Al_2O_3 atomic layer deposition for solid-state Li batteries. J. Electrochem. Soc. **159**(7), A1120 (2012)
55. Haruyama, J., Sodeyama, K., Han, L., Takada, K., Tateyama, Y.: Space-charge layer effect at interface between oxide cathode and sulfide electrolyte in all-solid-state lithium-ion battery. Chem. Mater. **26**(14), 4248–4255 (2014)
56. Otoyama, M., Ito, Y., Hayashi, A., Tatsumisago, M.: Raman imaging for $LiCoO_2$ composite positive electrodes in all-solid-state lithium batteries using Li_2S–P_2S_5 solid electrolytes. J. Power Sources **302**, 419–425 (2016)
57. Wang, H., Rus, E., Sakuraba, T., Kikuchi, J., Kiya, Y., Abruña, H.D.: CO_2 and O_2 evolution at high voltage cathode materials of Li-ion batteries: a differential electrochemical mass spectrometry study. Anal. Chem. **86**(13), 6197–6201 (2014)
58. Auvergniot, J., Cassel, A., Ledeuil, J.B., Viallet, V., Seznec, V., Dedryvere, R.: Interface stability of argyrodite Li_6PS_5Cl toward $LiCoO_2$, $LiNi_{1/3}Co_{1/3}Mn_{1/3}O_2$, and $LiMn_2O_4$ in bulk all-solid-state batteries. Chem. Mater. **29**(9), 3883–3890 (2017)

59. Zhang, W., Leichtweiß, T., Culver, S.P., Koerver, R., Das, D., Weber, D.A., Zeier, W.G., Janek, J.: The detrimental effects of carbon additives in $Li_{10}GeP_2S_{12}$-based solid-state batteries. ACS Appl. Mater. Interfaces **9**(41), 35888–35896 (2017)
60. Chu, I.H., Nguyen, H., Hy, S., Lin, Y.C., Wang, Z., Xu, Z., Deng, Z., Meng, Y.S., Ong, S.P.: Insights into the performance limits of the $Li_7P_3S_{11}$ superionic conductor: a combined first-principles and experimental study. ACS Appl. Mater. Interfaces **8**(12), 7843–7853 (2016)
61. Sumita, M., Tanaka, Y., Ohno, T.: Possible polymerization of PS4 at a Li_3PS_4/$FePO_4$ interface with reduction of the $FePO_4$ phase. J. Phys. Chem. C **121**(18), 9698–9704 (2017)
62. Liu, Z., Fu, W., Payzant, E.A., Yu, X., Wu, Z., Dudney, N.J., Kiggans, J., Hong, K., Rondinone, A.J., Liang, C.: Anomalous high ionic conductivity of nanoporous β-Li_3PS_4. J. Am. Chem. Soc. **135**(3), 975–978 (2013)
63. Kim, K.H., Iriyama, Y., Yamamoto, K., Kumazaki, S., Asaka, T., Tanabe, K., Fisher, C.A., Hirayama, T., Murugan, R., Ogumi, Z.: Characterization of the interface between $LiCoO_2$ and $Li_7La_3Zr_2O_{12}$ in an all-solid-state rechargeable lithium battery. J. Power Sources **196**(2), 764–767 (2011)
64. Kim, H.S., Oh, Y., Kang, K.H., Kim, J.H., Kim, J., Yoon, C.S.: Characterization of sputter-deposited $LiCoO_2$ thin film grown on NASICON-type electrolyte for application in all-solid-state rechargeable lithium battery. ACS Appl. Mater. Interfaces **9**(19), 16063–16070 (2017)
65. Robinson, J.P., Kichambare, P.D., Deiner, J.L., Miller, R., Rottmayer, M.A., Koenig Jr., G.M.: High temperature electrode-electrolyte interface formation between $LiMn_{1.5}Ni_{0.5}O_4$ and $Li_{1.4}Al_{0.4}Ge_{1.6}(PO_4)_3$. J. Am. Ceram. Soc. **101**(3), 1087–1094 (2018)
66. Ohta, S., Kobayashi, T., Seki, J., Asaoka, T.: Electrochemical performance of an all-solid-state lithium-ion battery with garnet-type oxide electrolyte. J. Power Sources **202**, 332–335 (2012)
67. Peljo, P., Girault, H.H.: Electrochemical potential window of battery electrolytes: the HOMO–LUMO misconception. Energy Environ. Sci. **11**(9), 2306–2309 (2018)
68. He, T.T., Jing, M.X., Yang, H., Chen, H., Hua, S., Ju, B.W., Zhou, Q., Tu, F.Y., Shen, X.Q., Qin, S.B.: Effects of gelation behavior of PPC-based electrolyte on electrochemical performance of solid-state lithium battery. SN Appl. Sci. **1**(3), 1–8 (2019)
69. Sun, B., Xu, C., Mindemark, J., Gustafsson, T., Edström, K., Brandell, D.: At the polymer electrolyte interfaces: the role of the polymer host in interphase layer formation in Li-batteries. J. Mater. Chem. A **3**(26), 13994–14000 (2015)
70. Zhou, Q., Ma, J., Dong, S., Li, X., Cui, G.: Intermolecular chemistry in solid polymer electrolytes for high-energy-density lithium batteries. Adv. Mater. **31**(50), 1902029 (2019)
71. Seki, S., Kobayashi, Y., Miyashiro, H., Usami, A., Mita, Y., Terada, N.: Improvement in high-voltage performance of all-solid-state lithium polymer secondary batteries by mixing inorganic electrolyte with cathode materials. J. Electrochem. Soc. **153**(6), A1073 (2006)
72. Seki, S., Kobayashi, Y., Miyashiro, H., Yamanaka, A., Mita, Y., Iwahori, T.: Degradation mechanism analysis of all-solid-state lithium polymer secondary batteries by using the impedance measurement. J. Power Sources **146**(1–2), 741–744 (2005)
73. Zheng, J., Zheng, H., Wang, R., Ben, L., Lu, W., Chen, L., Chen, L., Li, H.: 3D visualization of inhomogeneous multi-layered structure and Young's modulus of the solid electrolyte interphase (SEI) on silicon anodes for lithium-ion batteries. Phys. Chem. Chem. Phys. **16**(26), 13229–13238 (2014)
74. Liu, T., Lin, L., Bi, X., Tian, L., Yang, K., Liu, J., Li, M., Chen, Z., Lu, J., Amine, K., Xu, K.: In situ quantification of interphasial chemistry in Li-ion battery. Nat. Nanotechnol. **14**(1), 50–56 (2019)
75. Wenzel, S., Leichtweiss, T., Krüger, D., Sann, J., Janek, J.: Interphase formation on lithium solid electrolytes-an in-situ approach to study interfacial reactions by photoelectron spectroscopy. Solid State Ion. **278**, 98–105 (2015)
76. Wood, K.N., Steirer, K.X., Hafner, S.E., Ban, C., Santhanagopalan, S., Lee, S.H., Teeter, G.: Operando X-ray photoelectron spectroscopy of solid electrolyte interphase formation and evolution in $Li_2SP_2S_5$ solid-state electrolytes. Nat. Commun. **9**(1), 1–10 (2018)
77. Chen, R., Li, Q., Yu, X., Chen, L., Li, H.: Approaching practically accessible solid-state batteries: stability issues related to solid electrolytes and interfaces. Chem. Rev. **120**(14), 6820–6877 (2019)

78. Wang, C., Zhao, Y., Sun, Q., Li, X., Liu, Y., Liang, J., Li, X., Lin, X., Li, R., Adair, K.R., Zhang, L.: Stabilizing interface between $Li_{10}SnP_2S_{12}$ and Li metal by molecular layer deposition. Nano Energy **53**, 168–174 (2018)
79. Han, X., Gong, Y., Fu, K.K., He, X., Hitz, G.T., Dai, J., Pearse, A., Liu, B., Wang, H., Rubloff, G., Mo, Y.: Negating interfacial impedance in garnet-based solid-state Li metal batteries. Nat. Mater. **16**(5), 572–579 (2017)
80. Hao, X., Zhao, Q., Su, S., Zhang, S., Ma, J., Shen, L., Yu, Q., Zhao, L., Liu, Y., Kang, F., He, Y.B.: Constructing multifunctional interphase between $Li_{1.4}Al_{0.4}Ti_{1.6}(PO_4)_3$ and Li metal by magnetron sputtering for highly stable solid-state lithium metal batteries. Adv. Energy Mater. **9**(34), 1901604 (2019)
81. Ohta, N., Takada, K., Sakaguchi, I., Zhang, L., Ma, R., Fukuda, K., Osada, M., Sasaki, T.: $LiNbO_3$-coated $LiCoO_2$ as cathode material for all solid-state lithium secondary batteries. Electrochem. Commun. **9**(7), 1486–1490 (2007)
82. Zhang, Z., Zhang, Q., Shi, J., Chu, Y.S., Yu, X., Xu, K., Ge, M., Yan, H., Li, W., Gu, L., Hu, Y.S.: A self-forming composite electrolyte for solid-state sodium battery with ultralong cycle life. Adv. Energy Mater. **7**(4), 1601196 (2017)
83. Liu, L., Qi, X., Ma, Q., Rong, X., Hu, Y.S., Zhou, Z., Li, H., Huang, X., Chen, L.: Toothpaste-like electrode: A novel approach to optimize the interface for solid-state sodium-ion batteries with ultralong cycle life. ACS Appl. Mater. Interfaces **8**(48), 32631–32636 (2016)
84. Hayashi, A., Masuzawa, N., Yubuchi, S., Tsuji, F., Hotehama, C., Sakuda, A., Tatsumisago, M.: A sodium-ion sulfide solid electrolyte with unprecedented conductivity at room temperature. Nat. Commun. **10**(1), 1–6 (2019)

Chapter 8
Advanced Characterization Techniques to Unveil the Dynamics of Challenging Nano-scale Interfaces in All-Solid-State Batteries

K. P. Abhilash, P. Sivaraj, Bhupendar Pal, P. Nithyadharseni, B. Nalini, Sudheer Kumar Yadav, Robert Illango, and Zdenek Sofer

K. P. Abhilash (✉) · B. Pal · Z. Sofer (✉)
Department of Inorganic Chemistry, University of Chemistry and Technology Prauge, Technická 5, 166 28, Prague 6, Czech Republic
e-mail: karuthea@vscht.cz

Z. Sofer
e-mail: Zdenek.Sofer@vscht.cz

B. Pal
e-mail: palh@vscht.cz

P. Sivaraj
Bavarian Center for Battery Technology, Macromolecular Chemistry II, University of Bayreuth, Universitätsstrasse 30, 95440 Bayreuth, Germany

P. Nithyadharseni
Institute for the Development of Energy for African Sustainability (IDEAS), College of Science, Engineering, and Technology, University of South Africa, Florida Science Campus, Roodepoort 1709, South Africa
e-mail: Palann@unisa.ac.za

B. Nalini
Department of Physics, Avinashilingam Institute for Home Science and Higher Education for Women, Coimbatore, Tamilnadu 641 043, India
e-mail: jyothsnalalin@gmail.com

S. K. Yadav
Eduard-Zintl-Institut für Anorganische und Physikalische Chemie, Technische Universität Darmstadt, Alarich-Weiss-Straße 12, 64287 Darmstadt, Germany

R. Illango
Institute for Energy Studies, Grand Forks, ND, USA
e-mail: roberti.pushparaj@und.edu

N. Palaniyandy et al. (eds.), *Solid State Batteries*, Advances in Material Research and Technology, https://doi.org/10.1007/978-3-031-12470-9_8

8.1 Introduction

The All-Solid-State Batteries (ASSBs) are considered as the next generation vital energy storage source for a myriad of applications from micro-electronics to Hybrid Electric Vehicles (HEVs). The commercial progression of ASSBs appeals to the complete understanding of the chemistry of the component materials that deploy as the electrode and solid electrolyte of the batteries. There are two critical solid–solid interfaces in ASSBs; Cathode–Solid Electrolyte (SEs) and Anode: Solid electrolyte. The solid–solid interfaces of the ASSBs are critical owing to the failure in facile ion transfer through the interface results in a complete breakdown of the battery [1, 2]. Hence a clear understanding of the ASSB interfaces are highly important to visualize an ASSB with an electrochemical performance that can satisfy the industrial world for its eclectic commercialization.

The solid–solid interfaces of ASSBs are limited by some of the major issues such as the dendrite formation at the region of the interface (which can breakdown the battery performance), space charge layer formation due to the accumulation of charges (which can block the ionic movement through the interface), interface non-compatibility due to the surface mismatch and loss of contact at the interface region, which can lead to the high resistance layers that can damage the battery performances [2, 3]. Hence the solid–solid interface becomes the crucial point for better electrochemical performance in ASSBs. The inclusive knowledge about the possible chemical composition at the region of interface and other different interfacial phenomena are highly desired to design suitable interfaces with facile ionic migration.

A clear understanding of the interfacial phenomena is highly difficult owing to the lack of proper instrumentation available to probe it in the most accurate way [4]. The button type cell results in a thick layer of cathode (active material), solid electrolyte, and anode, in which the interfacial layer lies deep inside the surface layer. This demands the probing instruments to probe deep layer phenomena with highest accuracy [5]. This again limits the available instruments since most of the instruments probe only the surface thin layer of the samples. Some of the researchers shed light in to the role of developing advanced characterization techniques for ASSB interfaces [6, 7].

The very high impedance value that developed at the region of the interface in solid–solid interface is one of the perplexing dilemma in the scientific world. This may derive from a series of reasons such as some unwanted subsidiary chemical reactions that occur before or during the charge–discharge process across the interface, space charge layer that developed across the interface (the true reason for the space charge formation is still under active investigations), lack of intimate interface electrode–solid electrolyte contact, un-favorable Solid Electrolyte Interface (SEI) layer formations and so on. Basically, the ionic transport in the solid–solid interfaces is entirely different from the solid–liquid interfaces. The liquid electrolytes have increased free volume and thus the ions can easily move as compared with solid electrolytes due to the screening effect as well as the surface nature (see Fig. 8.1).

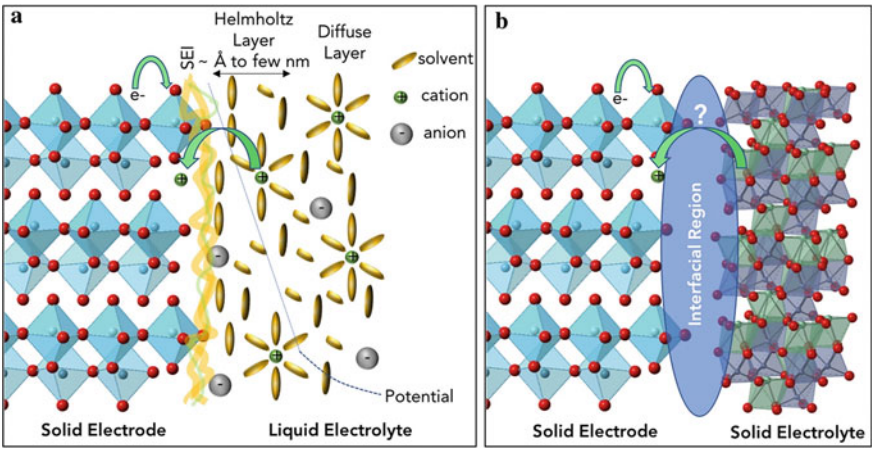

Fig. 8.1 The atomic level interfacial charge transfer at solid electrode-non-aqueous liquid electrolyte interfaces (**a**) and solid electrode/solid electrolyte interface (**b**) in energy Storage systems. Reprinted from reference [8], with permission from Elsevier, copyright (2018)

Screening ability at the interface can be realized by the Debye length, ion valence, and dielectric value of the electrolyte [8]. The knowledge about the charge transfer and interfacial mechanism at solid/solid interfaces are very less than that of solid/liquid interfaces [8].

In the field of ASSB analysis, a lot of innovative methods have been established over the past years to enlarge the capacity of understanding the essential structure–property-performance relationships at the nano-scale [9]. Different microscopic analysis/mapping methods, In-situ type characterization techniques, and Operando analysis methods are some of the most generalized technique that gives some vital information about the ASSB solid–solid interfaces. The separation of SEs from the electrode material causes harm to the interphase layers formed. This makes the in-situ spectroscopic techniques to be explored more in ASSBs [10].

The in-situ/operando characterization delivers the information regarding the interfaces when the reactions are in process. The terminology like ex-situ and in-situ are quite common to specify the way of characterization carried out for the sample. Ex-situ mode specifies that the sample is characterized outside the conditions that manifest the formation of the sample [11, 12]. In this case, most probably the characterization will carry out before or after the specified reaction to be carried out. In-situ mode, on the other hand, the characterization of the sample takes place at the same place with the similar condition of the reaction that occurs. The in-situ devices are often required to maintain an inert environment and low-pressures, and should be able to perform complete analysis without forfeiting the spatial resolution [9]. The in-situ electrochemical techniques are highly desirable to study the interfaces in solid-state systems [13]. On the other hand, operando is an in-situ method, wherein the characterization occurs when the device is in operating conditions. The in-situ and operando conditions are considered as two important ways to probe the precise

interfacial phenomena at nano-scale. Still, the lack of instrumentation/knowledge to effectively utilize the available instrumentation is the major difficulty faced by the researchers in the field of ASSBs, which retard the development of the technology to a large extent. It often requires custom device setup and is highly dependent on the chemistry and thermodynamic nature of the system. The macroscale analysis of the electrodes and solid electrolyte materials in ASSBs are not sufficient to uncover the dynamics of the solid–solid interfaces in ASSBs. The interfacial electrochemical properties of the solid–solid interfaces are in the nano-scale which are not well understood, by the macroscopic analysis technique. The atomic level structural and morphological information to probe the dynamics of the solid-state interfaces are still necessary for advancing ASSB technology. The improved understanding of the interface by the sophisticated instrumentation is the need of the hour.

8.2 State of the Art Interface Characterization Techniques

The interfacial compatibility in ASSBs are far less than that of the batteries that used organic liquid electrolytes [7]. The interface contact in liquid electrolyte batteries are highly intimate so that the ionic transfer becomes highly easy through the interface. But in the case of solid electrolytes the surface mismatch between the solid–solid surfaces makes it difficult to form an intimate contact between the electrode/electrolyte surfaces. This will result in an increase in the total impedance at the region of the interface of the ASSBs [14]. The interfacial side reactions further deteriorate the electrochemical performances by increasing the impedance for the ionic transport through the interface layers. The interfacial side reaction products that are deposited at the interface region makes additional impediment for the ionic movement [15]. The deep situated interface layer of the ASSBs makes it far from the reach of X-rays and IR radiations to probe out the region of the interface. This necessitates the sophisticated instrumentation for the precise interfacial characterizations of ASSBs. The different modifications of the conventional techniques based on electron microscopic, X-ray spectroscopic, optical, magnetic, and electrochemical principles, deserve special attention for the advanced interfacial modifications in ASSBs.

8.2.1 Electron Microscopic Techniques

The electron microscopy based techniques such as Scanning Electron Microscopy (SEM) and Transmission Electron Microscopy (TEM) paved the way to understand the finest information about the morphological evolution of the interface. This helps to leverage the particle sizes, microstructural evolution, and kinetics of the involved chemical processes at the region of the interface [16].

The Transmission Electron Microscopy (TEM), like Scanning Electron Microscopy (SEM) is a technique developed to obtain a better magnification and resolution than a conventional light microscope by using a focused beam of high energy electrons. The de Broglie wavelength of the electron makes it possible to get thousand times better resolution than a light microscope and enables to examine fine details [17]. It can give morphological information of the shape and size of particles in a microstructure. It can also reveal the nature of crystallographic defects present in the sample. The possibility for high magnifications has made the TEM a valuable tool in both medical, biological, and materials research, especially in the nano-research scenario. The TEM is a powerful microscope capable of producing images with 1 nm in size. Transmission Electron Microscope images the transmission of a focused beam of electrons through a sample to constitute an image. When an electron beam passes (transmitted) through a thin-section of a material, electrons may interact with the specimen to give the fingerprint of the surface layer under investigation.

The Scanning Electron Microscopy (SEM) is also a method for high-resolution imaging of surfaces. The SEM uses electrons for imaging, much as a light microscope uses visible light. The advantage of SEM over light microscopy include much higher magnification (>100,000×) and greater depth of field up to 100 times that of light microscopy [18]. In SEM, an electron beam is scanned across the surface of the specimen, which must be conducting. Back scattered electrons are collected and displayed at the same scanning rate on a cathode ray tube. The result is an image, much like a television image containing the surface features of the specimen. This image has a very great depth of field so that even a fractured surface without any polishing can be imaged.

Accelerated electrons in SEM carry significant amounts of kinetic energy and this energy is dissipated as a variety of signals produced by electron sample interactions when the incident electrons are decelerated in the solid sample. These signals include secondary electrons, backscattered electrons, diffracted backscattered electrons (that are used to determine crystal structures and orientations of minerals), photons (characteristics X-rays that are used for elemental analysis and continuum X-rays), visible light (Cathode Luminescence—CL) and heat [19].

The SEM analysis is an interface analysis tool that finds a lot of merits. The SEM can be utilized as different modes of operation since the electron sample interaction can produce not only the diffracted electrons but secondary electrons, photons, back scattered electrons, and so on. Hence this principle makes the possibility to use an SEM vacuum chamber to couple with different spectroscopic analysis such as back scattering spectroscopy, mass spectroscopy, and different optical spectroscopies by attaching different optical microscopes, EDX spectroscopy and so on. This property makes SEM a more convenient tool as an interface analysis tool even when the level of magnification is low when compared with TEM.

The TEM gives up to 50 million magnification level while SEM only offers 2 million as a maximum level of magnification. The resolution of TEM is down to 0.5 angstroms while SEM has a resolution limited slightly below 0.5 nm. The magnification level of TEM ranges from ×200 to ×1,500,000 times the original image. The

interaction of these electron beams with the material probes the morphology of the surface and elemental composition. The TEM can be utilized as a powerful tool to analyze the exact particle distribution, size of the particles or layers, and its orientation. The TEM can be utilized to analyze the morphology of the ASSB interfaces in the most precise manner. The TEM instrument attached with EDX spectra can be utilized to analyze the elemental compositions and exact stoichiometry.

The in-situ TEM characterization can clearly probe out the morphological, elemental, and structural evolution of the interface of ASSBs. The TEM is considered as a device which allows to couple with many other instruments in an easy way. The TEM analysis technique when attached with an electron energy loss spectroscope (EELS) [20], X-ray energy dispersive spectrometer (EDS) [21, 22], and high-angle annular dark field (HAADF) [5, 23] can analyze the elements that present at the region of interface, changes, distribution of the elements at the region of interface and the identification of different phases that is present at the region of the interface. The EDX analysis cannot detect elements with lower atomic numbers below Carbon. The major demerits of EDX analysis in energy research is its inefficiency to identify or map Li content that is present in the sample. The electron energy loss spectroscopy, on the other hand, can identify the elements with a lower atomic number in a more precise manner [20].

In the usual TEM the images are collected from the thin surface layer. The Scanning Transmission Electron Microscope (STEM) on the other hand, the beam of electrons will concentrate on a fine spot (up to 0.2 nm) and then scan over the surface by a raster illumination system. The STEM is basically a TEM with more number of scanning coils and additional detectors. Coupling STEM with EDS, Sakuda et al. analyzed the formation of the SEI layer and the diffusion of Co, P, and S formed at the Lithium Cobalt Oxide/Solid Electrolyte interface after charging [23]. In an operando STEM coupled with EELS analysis, Nomura et al. elucidate the interfacial phenomena and Li ion distribution of ASSBs [24]. The study attempts to probe the interfacial phenomena on a nanometer scale. The quantitative Li ion distribution within and across the interfacial regions could be possible with the STEM coupled with the EELS technique in the operando condition. The study predicts that the STEM-EELS analysis could predict the inactive layers present in the sample after charging. The $LiCoO_2/Li_2O–Al_2O_3–TiO_2–P_2O_5$ interface after charging develops an inactive region with 10–20 nm thickness containing the mixture of $LiCoO_2$ and Co_3O_4, leading to the higher interfacial resistance for the Li ion transfer (Fig. 8.2). This inactive interfacial layer causes the additional interfacial resistance with blocked Li ion diffusion pathways across the interfacial region. The combination of elemental analysis techniques like EDX or EELS with the STEM can disclose the interfacial phenomena, bonding characteristics, and the mechanism of degradation in ASSBs.

Wang et al. also tried to unravel the interfacial phenomena during the Li ion transfer through a quantitative spectroscopic analysis of the interfacial layer between $LiCoO_2$ cathode and LiPON electrolyte in an in-situ galvanostatic electrochemical system [25]. The spectroscopic analysis showed that one disordered interfacial layer has been formed from the structurally unstable cathode materials in highly de-lithiated states. The layer formed between cathode and electrolyte accumulates lithium, with the

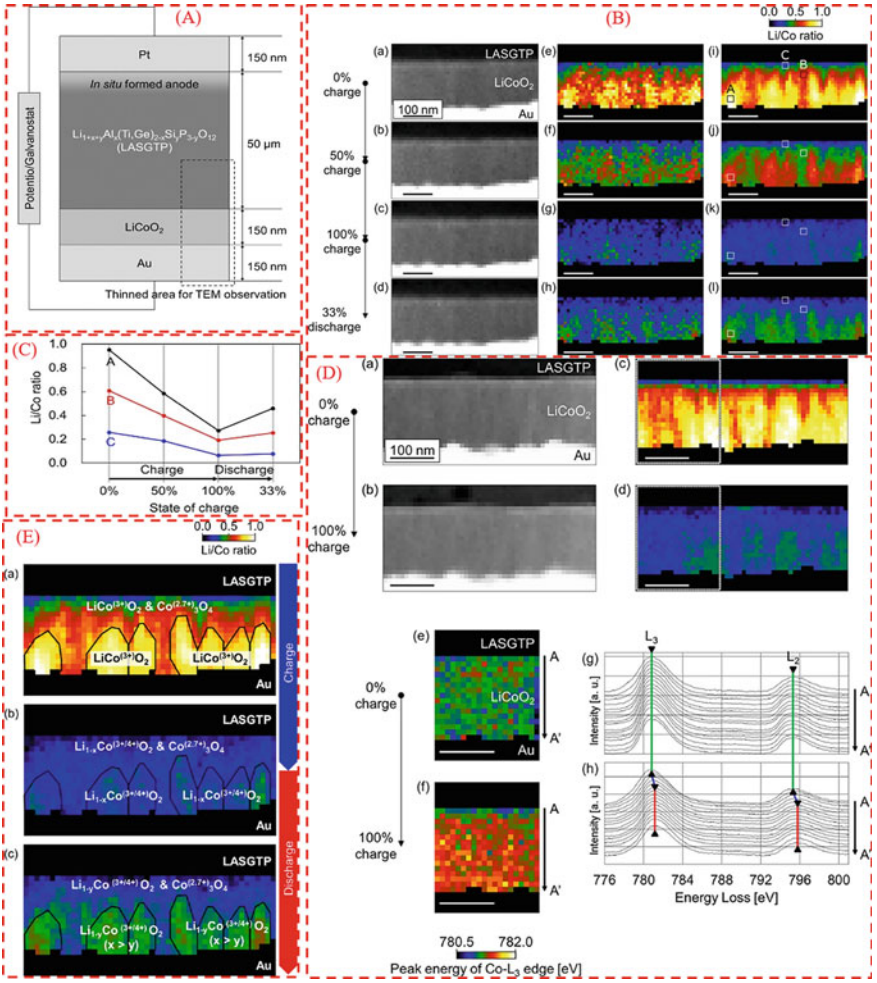

Fig. 8.2 The operando STEM coupled with EELS analysis elucidating the formation of an inactive interfacial layer and Li ion distribution in ASSBs; (**A**) Cell configuration (**B**) The Li ion distribution by operando STEM-EELS analysis by hyperspectral image analysis of non-negative matrix factorization (NMF). (**a–d**) The images of ADF-STEM at 0, 50, 100% charged and 33% discharged states, respectively. (**e–l**) The Li/Co ratio maps obtained from (**e–h**) original (**i–l**) NMF-reconstructed SIs; (**C**) Plots of a Li/Co ratio at A, B, and C regions in panels (**i–l**). (**D**) Operando STEM-EELS analysis for the valence changes in Co ion. (**a** and **b**) The ADF-STEM images at 0 and 100% charged states and (**c** and **d**) corresponding NMF-reconstructed Li/Co ratio maps. (**e** and **f**) Mapping of the peak position of the Co-L3 edge at the dotted box in panels c and d. Brighter color indicates higher energy loss in the EEL. (**g** and **h**) spatially resolved 1D-EEL spectra of Co-L2,3 from A to A in panels e and f. Lines green, blue, and red show the peak energies of each Co-L2,3 edge. (**E**) Li map and composition in the cathode film at (**a**) 0% charged state, (**b**) 100% charged state, and (**c**) 33% discharged state. The black lines surrounded regions show the $LiCoO_2$ grains and other regions show the mixture of Co_3O_4 and $LiCoO_2$, where Co_3O_4 is concentrated near the LASGTP side rather than the Au side. Reprinted from reference [24], with permission from Elsevier, copyright (2018)

formation of intermediate compounds at the region of the interface (like Li_2O/Li_2O_2), making the cathode electrochemically inactive. This sophisticated interfacial analysis suggests that the increase in the interfacial impedance at the $LiCoO_2$/LiPON interface is triggered by chemical changes instead of space charge effects [25].

8.2.2 X-ray Based Techniques for the Interface Analysis

The X-ray based techniques such as X-ray diffraction (XRD) [26] X-ray tomography, X-ray absorption spectroscopy (XAS), and X-ray absorption near-edge spectroscopy (XANES) have been used to expose the structural information in the material systems [27]. When an X-ray beam hits an atom, the electrons around the atom start to oscillate with the same frequency as the incoming beam. The reflected, backscattered beam has the figure print of the surface of co-incidence of the X-rays.

The X-ray Diffraction (XRD) analysis is the most powerful tool for the structural analysis for ever. When an X-ray beam hits an atom, the electrons around the atom start to oscillate with the same frequency as the incoming beam. Braggs' law states that the incident X-ray radiation would produce a Bragg peak if the reflections of the various planes interfered constructively. Mainly the in-situ XRD technique has been preferred for the interface analysis of the ASSBs. In recent years, X-ray photoelectron spectroscopy (XPS), X-ray tomography, and X-ray absorption spectroscopy (XAS) have established the prominence in the characterization of the ASSB interfaces.

The X-ray absorption spectroscopy (XAS) utilizes the synchrotron radiation source which can produce different kinds of X-rays. After absorbing the radiation the atoms in the sample and the scattering of this radiation produces the photo electrons. The XAS is a technique in which fast and precise measurement of the electronic environment of the atoms in the samples is possible. The XAS and XPS, are the chemical element characterization and concentrations analysis techniques. The XPS can detect 10 nm, while XAS detects 100 nm of the sample [5].

The X-ray absorption near-edge spectroscopy (XANES) has been developed as an information tool on the chemical state of the elements and the local electronic structure of the battery materials [28, 29]. The XANES study in operando mode of analysis elucidates the electrochemical reactions that occur in the interfaces and the formation of intermediate reaction products. The XANES studies can be coupled with different other characterization techniques such as high-angle annular dark field (HAADF) and scanning transmission electron microscopy (STEM) with electron energy loss spectroscopy (EELS) to elucidate the interface development during the charge/discharge process.

Li et al. carried out an operando XANES combined with TEM and EELS to investigate the commercial Ni-rich $LiNi_{0.8}Mn_{0.1}Co_{0.1}O_2$ (NMC811) cathode and $Li_{10}GeP_2S_{12}$ (LGPS) solid electrolyte [28]. The study also tries one interface coating strategy with ultrathin thick lithium niobium oxide (LNO) to alleviate the interfacial impedance. The study clearly establishes the role of an operando XANES approach in comparison with the ex-situ XANES method to unravel the interfacial parasitic

side reactions that involve the metastable phase. The study reveals that the contact of non-coated NMC811 and LGPS induces parasitic interfacial reactions with the formation of a metastable intermediate state during the initial charging process, especially at high voltage. This result, in the formation of Li_2S impurity phase by the LGPSs decomposing, causing the microstructure cracks and degradation at the surface of NMC811 cathode particles. The accumulation of the products from this parasitic reaction that are accumulated at the interface results in a large irreversible capacity loss and performance degradation. The LNO coating helps to protect the NMC811 cathode and stabilize the interface between leading to promising cycling performance of the cathode in SSLIBs (Fig. 8.3).

The X-ray tomography can map the 3D structure of the samples and the deep layers of the electrode/electrolyte or the interfaces of the ASSBs. The time-resolved X-ray tomography can be utilized to probe the changes in the morphology of the analyzing surface in a systematic manner. The analysis of the interfacial region or the electrode/electrolyte material after prolonged cycling provides information about the structural or morphological degradation of the electrode and electrolyte materials of the ASSB assembly. The microstructural and minute morphological information of the interfaces using the X-ray tomographic technique in operando or in-situ mode is possible by properly upgrading the instrument in different ways.

8.2.2.1 X-ray Photo Electron Spectroscopy for Interface Analysis

The X-ray Photo electron spectroscopy (XPS) is considered to be one of the best characterization techniques for precise elemental analysis. The excitation of photons using the X-ray source to emit the electron from the sample by its ionization technique, has been utilized as the principle in XPS elemental analysis technique. The precise quantitative and qualitative elemental determination makes XPS one of the finest characterization techniques for stoichiometric analysis of the samples. The presence of Lithium metals which are highly important in LIB characterizations and usually difficult to detect using the Energy dispersive X-ray (EDX) measurement can be detected in XPS analysis. The overlapping spectral lines that occur in the EDX measurement for numerous elements in the periodic table make it less accurate in some precise measurements. But the XPS can clearly differentiate the elements with overlapping spectral lines, which makes the precise measurement of the sample in more sensitive way. The XPS is a more sensitive technique to measure even some trace amounts of the samples that are present in a mixture. The sampling depth of XPS ranges from 3 to 10 nm, which makes it suitable for the depth profile analysis of the sample. The researchers suggest that the XPS is one of the best methods for interface elemental analysis in ASSBs.

The XPS technique is helpful in analyzing the individual elemental compositions of the electrode and electrolyte materials employed in ASSB assemblies. Along with this, the major advantage of this method is the precise quantitative and qualitative identification of the elements present in the interfacial layers. The measurement of

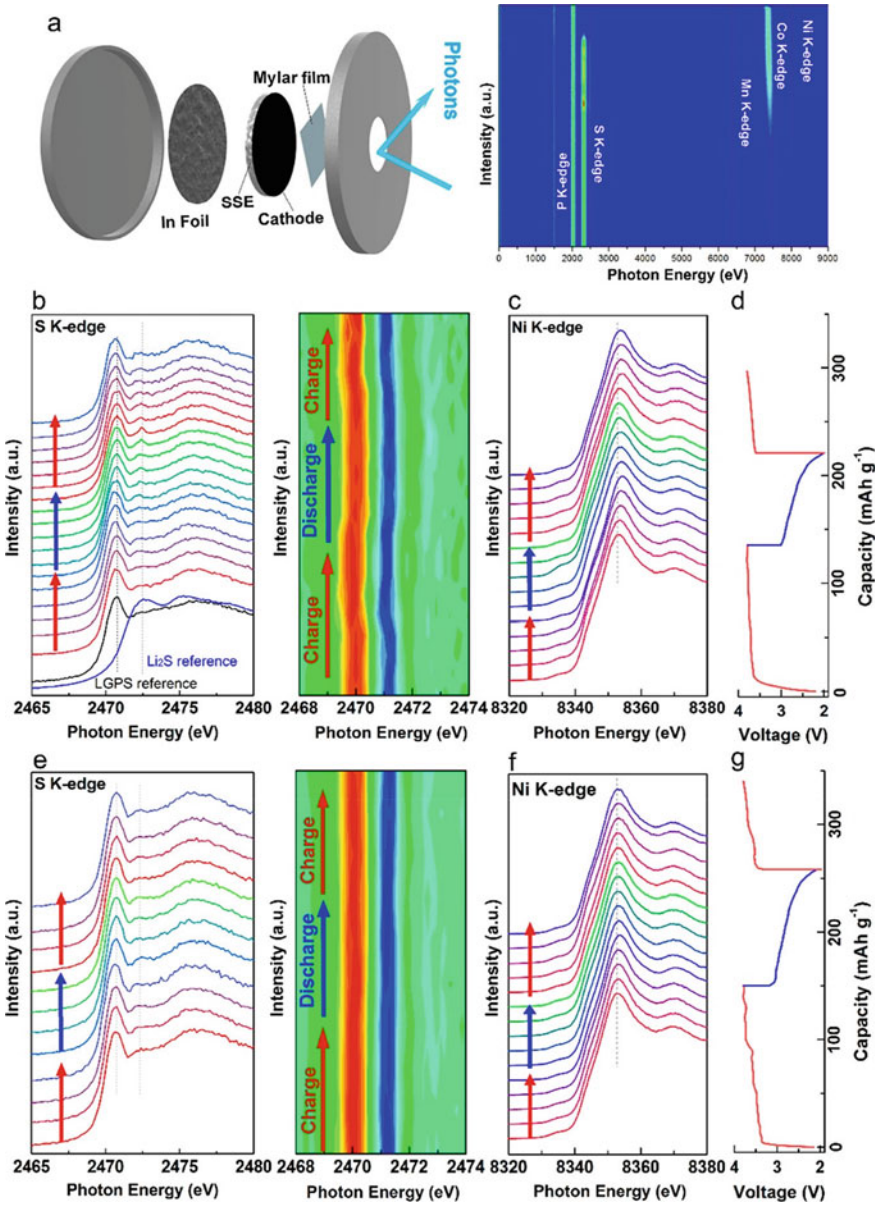

Fig. 8.3 The operando XANES study in ASSB interfaces between $LiNi_{0.8}Mn_{0.1}Co_{0.1}O_2$ (NMC811) cathode and $Li_{10}GeP_2S_{12}$ (LGPS) solid electrolyte with and without lithium niobium oxide (LNO) coating; (**a**) schematic of the assembly of operando cell and the obtained Bruker spectrum of large photon energy region. S K-edge spectra with first derivative mapping (**b**), Ni K-edge spectra (**c**), and charge/discharge profiles (**d**) of bare NMC811-LGPS in operando mode and the respective spectrums in LNO coated NMC811-LGPS SSLIBs (**e–g**). Reprinted from reference [28], with permission from American Chemical Society, Copyright © 2019

elemental compositions at the region of interface clearly verifies the formation of Solid Electrolyte Interface (SEI) layers.

The in-situ XPS analysis is considered as one of the powerful tools to analyze the interface formation in ASSBs. The elemental composition at the region of the interface of ASSBs can be analyzed at the time of interface formation which will shed light in to the interface subsidiary reactions that lead to the additional impediment of the ASSB interfaces. The in-situ XPS analysis is a tedious process since the interface formation has to be verified in a vacuum chamber either inside the XPS chamber or attached with the XPS instrument.

In one of the attempts by Auvergniot et al., the XPS analysis has been performed at different depths to characterize the deeper interfacial layers in the all-solid-state half-cells of $LiCoO_2/Li_6PS_5Cl/Li–In$, $LiNi_{1/3}Co_{1/3}Mn_{1/3}O_2/Li_6PS_5Cl/Li–In$, and $LiMn_2O_4/Li_6PS_5Cl/Li–In$ systems, in pristine and cycled samples to study the interfacial stability of Argyrodite (Li_6PS_5Cl), against different cathodes (Fig. 8.4) [12]. The study reveals the formation of elemental sulfur, lithium polysulfides, P_2S_x ($x \geq 5$), phosphates, and LiCl due to the oxidation of Li_6PS_5Cl at the interface with the positive electrode active materials. The studies could uncover that the better electrochemical performance even when the oxidation of Argyrodite (Li_6PS_5Cl) solid electrolyte, derives from some reversible electrochemical activity of this subsidiary compounds that formed due to the oxidation.

The ASSB material characteristics even differ during the intercalation/de-intercalation of Li ions. The interaction properties of the Li ions or the elemental composition at different places during the intercalation is only possible by monitoring the charge–discharge characteristics of the batteries by XPS instrument. The technical limitation of the instrument stops the coupling of charge–discharge devices to couple with the XPS instrument. Even when, the XPS stands as a strong probing technique to analyze the interfacial elements with utmost precision in in-situ or ex-situ mode.

8.2.3 Optical Spectroscopic Techniques for the Interface Analysis

The optical microscopy can be utilized as a tool to monitor the interface reactions at the time of charging/discharging or after prolonged charge–discharge. The optical microscope can be attached with different other characterization tools that operate in in-situ or ex-situ mode to record the changes that occur at the region of interface during or after prolonged charge–discharge. Even though it is quite difficult to probe high magnification images using Optical microscopy, it is considered as a simple and cost effective method which can easily couple with many of the other battery characterization techniques. The optical analysis like Raman analysis and Fourier Transform Infrared Spectroscopy (FTIR) provide wide information on the surface chemistry [30].

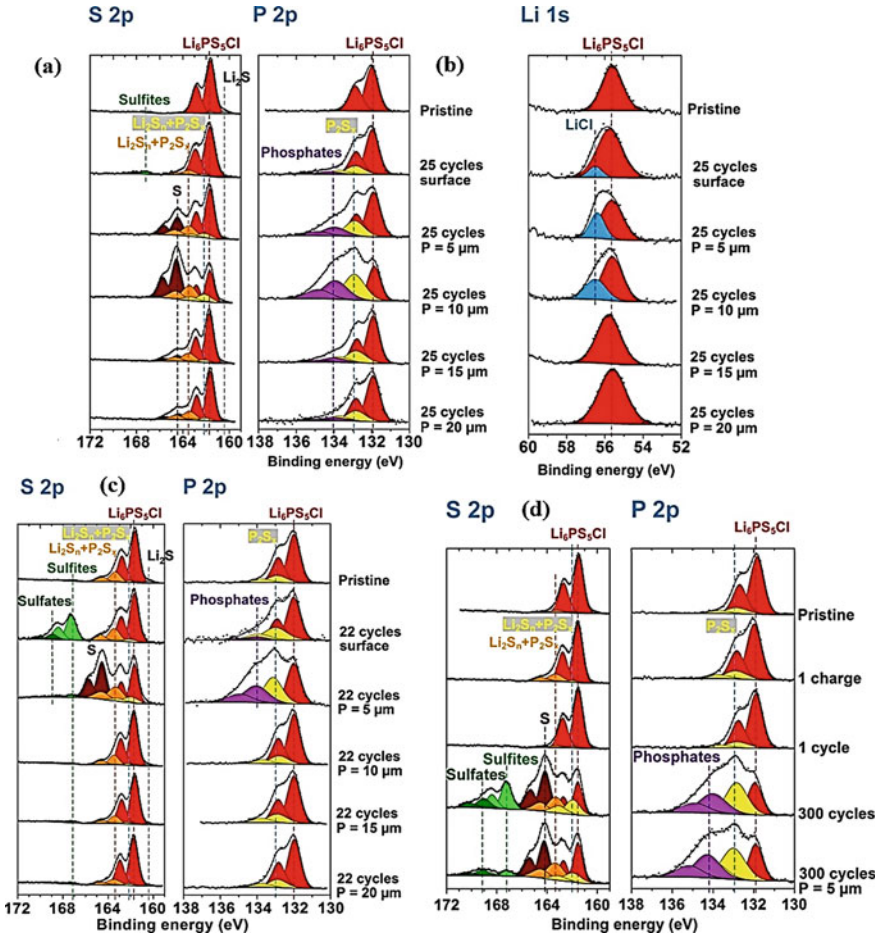

Fig. 8.4 The XPS analysis that performed at different depths to characterize the deeper interfacial layers in the all-solid-state half-cells of $LiCoO_2$ (LCO)/Li_6PS_5Cl/Li–In, $LiNi_{1/3}Co_{1/3}Mn_{1/3}O_2$ (NMC)/Li_6PS_5Cl/Li–In, and $LiMn_2O_4$ (LMO)/Li_6PS_5Cl/Li–In systems; (**a**) S 2p, P 2p and (**b**) Li 1s XPS spectra of LCO electrode in LCO/Li_6PS_5Cl/Li–In half-cells: pristine, after 25 cycles, and with increasing electrode etching depths from 5 to 20 μm after 25 cycles. (**c**) The S 2p and P 2p XPS spectra of LMO electrode in LMO/Li_6PS_5Cl/Li–In half-cells: pristine, after 22 cycles, and with increasing electrode etching depths from 5 to 20 μm after 22 cycles; (**d**) The S 2p and P 2p spectra of NMC electrode in NMC/Li_6PS_5Cl/Li–In half-cells: pristine, after the first charge, after one cycle, and after 300 cycles with and without electrode surface etching of 5 μm. Reprinted from reference [12] with permission from American Chemical Society, Copyright © 2019

The elastic or inelastic scattering of light photons that incident on the surface of some molecules has been first predicted by C. V. Raman. Raman spectroscopy is based on the Raman effect and is known to be one of the powerful techniques for the analysis of molecular vibrations and the functional groups holding in a compound. The molecular structural analysis and elemental analysis of the ASSB materials are possible by Raman analysis. The composition of the material can be analyzed from the characteristic peaks in the Raman spectra. Raman spectra can also analyze the polarization that occurred in the compound and the qualitative and quantitative analysis of the elements which is possible to probe relatively from the peak intensity and peak area.

There are many advantages for Raman analysis. It is a non-destructive technique and the analysis completes without any impairment to the sample. The measurement of samples is possible at high temperature and high pressure. At the interface region, if some changes in composition occur, that can be monitored by the Raman analysis technique. Raman spectroscopy gives some clear picture about the single, double, and triple bond formation in different compounds. This can be effectively used to analyze the composition change that occurs at the region of the interface during the cycling or after prolonged cycling. The in-situ Raman spectroscopy can be utilized properly to probe the interface region during the formation of the interface and during the Li ion intercalation. The Raman mapping can also be utilized to probe the elemental/molecular distribution at the interface region of ASSBs.

8.2.4 Magnetic Techniques for the Interface Analysis

Magnetic techniques like nuclear magnetic resonance (NMR), magnetic resonance imaging (MRI), and Mössbauer spectroscopy have been grasped to accomplish the quantitative and qualitative analysis of different elements present in the interface [31]. The Nuclear Magnetic Resonance (NMR) is a powerful tool to give information about the structure of the compounds at the region of the interface. The NMR records the nuclear resonance under the application of an external magnetic field. It is based on the principle of spinning of the nucleus under the external field. The nuclei after absorbing the characteristic frequency pulses in the external magnetic field release the NMR signals characteristic to the local environment. The NMR mainly gives the structural and chemical information related with the analyzing species. The NMR is considered to be one of the powerful tools to detect chemical processes that occurs during the intercalation–de-intercalation of the Li ions. The in-situ NMR can be utilized to probe the interfacial phenomena without any damage to the battery materials.

8.2.5 *Electrochemical Impedance Spectroscopy (EIS) as an Interface Analysis Tool*

Ionic and electronic transport is critical parameters for the solid electrolytes and the electrode–solid electrolyte interfaces, which are usually evaluated by electrochemical impedance spectroscopy (EIS). The Complex Impedance Spectroscopy (CIS) is the most elegant and powerful technique for the electrical characterization of solids, in general, and electrochemical devices including electrodes as well as electrolytes in particular. This technique is often used to obtain bulk conductivity, but additional information related to the motion of charged particles could also be obtained. It resolves the elementary hoping processes of mobile charges. In addition, it is a powerful technique to investigate interfaces [32].

In general, electrical characterizations can be done by DC and AC measurement techniques. Though the DC measurement technique is straightforward, it cannot be implemented for solid electrolytes for the following reason: (1) As the DC field is applied to the electrolyte, the material gets polarized and ionic conductivity ceases, giving only electronic conductivity; (2) It is difficult to find an electrode material compatible with the solid electrolyte that does not give polarization effects at the electrode–electrolyte interface. Therefore for solid electrolytes, AC measurement of electrical conductivity is done to avoid polarization of the sample.

On applying a sinusoidal voltage $V = V_{\max}\sin\omega t$, where ω $(2\pi f)$ is the angular frequency, a current will flow within the electrolyte with an identical frequency to that of the applied voltage. Due to capacitive and inductive effects, however, the current is typically out of phase with the voltage.

$$\text{i.e.,}\ \ I = I_{\max}\text{Sin}(\omega t + \theta) \tag{8.1}$$

where, $I_{\max}$ is the maximum current and θ is the phase angle. The relationship between applied voltage and resultant current can be written as:

$$Z = V_{\max}/I_{\max} \tag{8.2}$$

where, $V_{\max}$ is maximum voltage. Z is the total impedance or opposition to the charge flow within electrolyte. The admittance, the ease of charge flow through the material can be written as:

$$Y = 1/Z = I_{\max}/V_{\max} \tag{8.3}$$

With a phase difference between $V_{\max}$ and $I_{\max}$, the impedance and admittance are vector quantities, processing magnitude and phase and as such may be represented in the vector plane. Similarly, both quantities may be represented in the complex plane, where X and Y axes are designated as the real and imaginary components respectively.

Table 8.1 Interrelation between impedance parameters

Variable	M	Z	Y	ϵ^*
M	M	$j\omega C_0 Z$	$j\omega C_0 Y^{-1}$	ϵ^{*-1}
Z	$(j\omega C_0)^{-1} M$	Z	Y^{-1}	$(j\omega C_0)^{-1} \cdot \epsilon^{*-1}$
Y	$j\omega C_0 M^{-1}$	Z^{-1}	Y	$j\omega C_0 \cdot \epsilon^*$
ϵ^*	M^{-1}	$(j\omega C_0)^{-1} \cdot Z^{-1}$	$(j\omega C_0)^{-1} Y$	ϵ^*

$$Z* = Z'_{\text{real}} - -jZ''_{\text{imaginary}} \tag{8.4}$$

$$Y* = Y'_{\text{real}} - -jY''_{\text{imaginary}} \tag{8.5}$$

However to obtain a more accurate characterization of the material under study is often necessary to use two other formalisms, closely related to those mentioned above; i.e., the complex electric modulus and complex permittivity. They are given by

$$M = M'_{\text{real}} - M''_{\text{imaginary}} = j\omega C_0 Z* \tag{8.6}$$

$$\in ** = E'_{real} - E''_{imaginary} = (j\omega C_0)^{-1} Y* \tag{8.7}$$

where C_0 is the vacuum capacitance of the cell. The interrelationships between different impedance parameters are tabulated in Table 8.1.

In the electrochemical impedance analysis, an AC potential is applied to a solid electrolyte and the current through the sample is measured. The response to this potential is an AC current signal containing the excitation frequency and harmonics. By observing the current response, the resistance within different frequencies can be examined. The electrochemical impedance is measured from this small excitation signal and the data can be represented as a Nyquist plot as shown in Fig. 8.5.

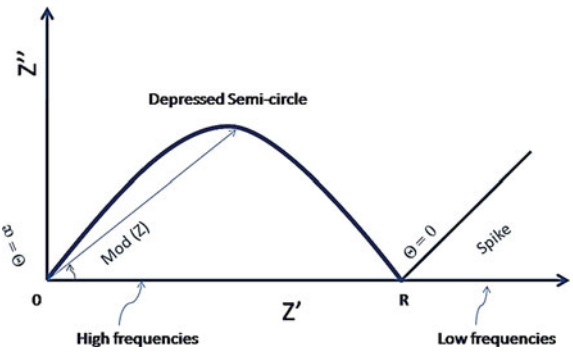

Fig. 8.5 A typical Nyquist plot

On the Nyquist plot, the impedance can be represented as a vector (arrow) of length |*Z*|. The angle between this vector and the X-axis, commonly called as the "phase angle", f (=arg *Z*). Another common representation is the Bode plot where the impedance is plotted with log frequency on the X-axis and both the absolute values of the impedance ($|Z|=Z_0$) and the phase-shift on the Y-axis. Unlike the Nyquist plot, the Bode plot gives the frequency information. The Nyquist plot could be fitted using an equivalent circuit called the Randles circuit made up of a series or parallel combination of resistors and capacitors. Each circuit element represents a component of the electrochemical cell and thus the model will stimulate the experimental impedance spectrum. The impedance spectrum can be divided into a high-frequency region (>1 MHz), a mid-frequency region (1 kHz–100 Hz), and a low-frequency region (~1 Hz), analogous to the resistance contributions from the bulk electrolyte, charge transfer, and Warburg diffusion, respectively.

Nyquist plot: The Nyquist or complex impedance plane plot is for evaluating electrochemical data. Here the plot is between Z' and Z'' of impedance data. This plot shows a slightly depressed semicircle which corresponds to the bulk resistance. The ionic conductivity can be determined from resistance where the semicircle crosses the X-axis. From the plot, one can infer about the polarization nature of the sample. For a material which obeys Debye law, the center of the semicircle lies exactly on the real axis and one can distinguish the Debye and non-Debye nature of the materials.

The frequency corresponding to the top of the semicircle ω_{max} can be used to calculate the capacitance, if R_b is known,

$$C_b = 1/2\pi\omega_{max}R_b \tag{8.8}$$

The electrical conductivity of the bulk electrolyte is obtained by

$$\sigma_0 = \frac{l}{A}(1/R_b) \tag{8.9}$$

where, A is the area of the sample, l is the thickness of the sample, and R_b is the bulk resistance. The bulk resistance can be determined from the Nyquist plot where the semicircles intercept on the Z' axis. Hence by using the Nyquist plot, the values of the relaxation time, the bulk capacitance of the sample can also be obtained.

Equivalent circuit modelling: of EIS data is used to extract physically meaningful properties of the electrochemical system by modelling the impedance data in terms of an electrical circuit composed of ideal resistors (R), capacitors (C), and inductors (L).

The generalized Constant Phase Element (CPE) and Warburg Element (Z_W) are also used to represent the diffusion or mass transport impedances of the cell. In the equivalent circuit analog, resistors represent conductive pathways for ion and electron transfer. Resistors are also used to represent the resistance to the charge transfer process at the electrode surface. Capacitors and Inductors are associated

with space charge polarization regions, such as the electrochemical double layer and adsorption/desorption processes at an electrode, respectively.

The EIS as an advanced interfacial characterization tool: The growth of degradation of the interface in ASSBs can be identified after the electrochemical cycling as an increase in cell resistance obtained by the EIS measurement [10]. The individual influences from different resistance developments can be differentiated by the EIS technique. The time-resolved EIS is considered as a powerful tool to identify the formation of interphase layers through changes in resistance and capacitance at the region of the interface [10]. EIS is considered as one of the most attractive and simple techniques to characterize the interface, which has been less explored by the scientific world. High level of theoretical knowledge is the most necessary component to analyze the interface data, since the equivalent circuit that is used to fit the impedance plots may not be relevant in physical intellect in some of the cases [33].

The Nyquist plot ($-Z''$ versus Z') of SEs manifests a series of semicircles which can be fitted using a series of parallel resistors and capacitors or constant phase elements (CPEs) [10]. The high-frequency regime corresponds to the bulk resistance. The middle-frequency regime was ascribed to the interfacial charge transfer resistance [34]. The lowest frequency region may manifest with a Warburg impedance in addition to the other components. A single electrode conductivity analysis probes the ionic transport component of the electrode/electrolyte material under investigation. The bulk and grain boundary components can be differentiated in many of the electrolyte/electrode materials when it is analyzed as a single component in the EIS analysis. In that case, the grain boundary component may result in an additional semicircle separated from the grain resistance.

The ionic movement across the solid–solid interfaces are complicated than the single phase ionic movements. In this case, different components that give the individual resistances has to be considered individually. Different resistive components when considering the interface can be anticipated as [35]. (1) Interfaces of the region without any change in the patterning style of atoms, that gives minimum resistance/reactance for the Li ion movement; This occurs at high-frequency region (10^{-2} to 10^{-4} Hz) and minimum capacitance ((10^{-14} to 10^{-11} F): Path (A) in Fig. 8.6a; (2) Interface between the regions that have different in-homogeneities that establish the electrode–electrolyte layer; This comprises the mismatch of lattice arrangements (due to different types of atoms, the local space charge effects and changes in the directionality (1D, 2D, 3D movements) of charge carriers); This lies at the intermediate frequency windows (10^{-3} to 10^{-5} Hz) contributing the blocking capacitance of the range 10^{-11} to 10^{-8} F; Path (B) in Fig. 8.6a; (3) Interface regions between different phases due to the difference in chemical composition: Here the impedance arises from the discrepancies in phase boundaries, interfacial layers formation, and the reactions that occurs across the electrode/electrolyte interface. This region offers highest impedance to the charge carriers. This lies at lower frequency windows (10^{-5} to 10^{-7} Hz) which comprise the capacitance in the range of 10^{-8} to 10^{-5} F Path (C) in Fig. 8.6a.

The EIS spectra can be extended with different other characterizations in attached or collective way. Our research group utilized the EIS measurement at different

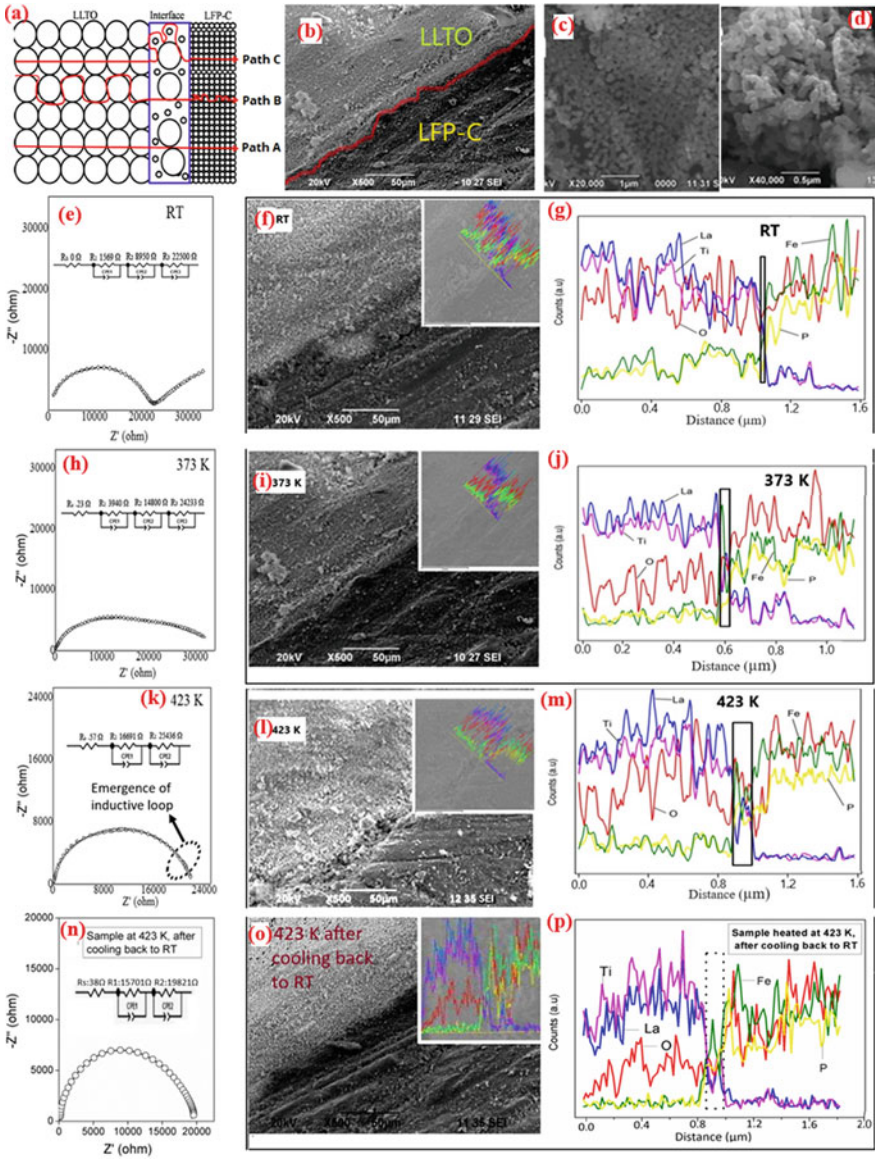

Fig. 8.6 The combined EIS, SEM, and EDX line mapping analysis to establish the increase in interface width at elevated temperatures in the LLTO/LFP–C interface (**a**) The schematic of different ionic conductivity mechanisms across the LLTO/LFP–C interface. The SEM micrograph of LLTO/LFP–C interface (**b**); LLTO (**c**) and LFP–C (**d**) samples. The conductivity, SEM, and Line mappings of the LLTO/LFP–C interface at RT (**e–g**), 373 K (**h–j**), 423 K (**k–m**) and 423 K: after cooling back to RT (**n–p**) respectively (Inset of SEM shows the combined image). Reprinted from reference [35] with permission from Elsevier, Copyright © 2019

temperatures to probe the ionic movement across the LLTO/LFP–C interface. Here the morphology and the elemental composition of the interface and across the interface has been analyzed at different temperatures. This ionic distribution data at different temperatures has collectively analyzed and compared with the fitted impedance plots at respective temperatures. The study reveals that the width of the interface region increases with the increase in the sintering temperature in the LLTO/LFP–C sample. The accumulation of heavier elements (La, Ti) at the region of interface is clearly evident by the line scan mapping (Fig. 8.6). This accumulation results in the increase in the interfacial width, which leads to the possible reason for the breakdown of interface in the ASSB assemblies with LLTO solid electrolytes. The thermodynamic instability is considered as one of the prominent reason for the interfacial instability in Solid–Solid interfaces in ASSBs [36]. The study can be extended for the charge–discharge process as well so that it can clearly probe the width of interface during the charge–discharge process in a simple ex-situ mode [35].

8.3 Other Promising Analysis Techniques to Unveil the Features of the All-Solid-State Interface

8.3.1 Neutron Depth Profiling

The major problem of the material scientists to analyze the interface characteristics is the lack of probing the depth profile. The interface layer in most of the cases situated deep from the exposed surface in ASSBs. Many of the instruments fail to probe the deeper layers since its inherent surface scanning methodology. Neutron Depth Profilling (NDP) technique can be utilized to determine the distribution of elements present about 1 μm below a surface layer. This can be attained by the neutron absorption of the substances under the irradiation of the neutron, which causes some exothermic reactions that triggers in some isotopes inside the materials. The NDP can be assumed as a powerful phase identification technique at deep below the surface layer. NDP can be utilized to analyze different phases that present at the region of interface in ASSBs.

8.3.2 Secondary Ion Mass Spectrometry

The Secondary Ion Mass Spectrometry (SIMS) is yet another powerful mapping tool for the deeper interfacial layers of ASSBs. The SIMS uses the secondary ions after the sample is excited by the primary ions. The SIMS can be utilized to identify different elements present in the deeper interfacial layers in ASSB assemblies. The SIMS can be modified in different way to obtain maximum information of the deeper layers of the sample. One of such modification is the Time of Flight Secondary Ion

Mass Spectrometry (TOFSIMS). The TOFSIMS can provide even the structural information of the elements present in the deeper layer by measuring the time of flight of the secondary ions that coming out of the deeper layer of the samples to the detector. It is considered as a sensitive technique to focus on the deeper layer of the sample to map the structure and composition in precise way.

8.3.3 Scanning Probe Microscopy Technique

The Scanning Probe Microscopy (SPM) based techniques are less explored for the electrochemical characterizations of the sample. This technique can be applied to investigate the electrochemical deformation of the sample on the nano-scale, under external bias voltage [37]. Zeng and his research group have devoted their research direction in expounding the electrochemical lattice strain due to the Li ion diffusion at different regions of the electrode and electrolyte materials of the ASSBs [38, 39]. The SPM techniques originated from the Scanning Tunneling Microscopy (STM), invented by Rohrer and Binnig [40]. The SPM techniques works under the principle of probing the surface by a sharp tip by positioning within a few nanometers over the surface and the signal of interaction is converted to a characteristic output signal using electronic circuitry with a piezo actuator [9]. They prove that this extended AFM technique can probe the electrochemical strain, Li ion distribution and activation energy of the electrode and electrolyte materials in ASSBs.

Over the past few years, SPM have delivered some fruitful solutions for addressing the scientific challenges through new characterization tools at the nano-scale [9]. The SPM is considered as one of the powerful techniques to characterize the interfaces of ASSBs at the nano-scale. The SPM deserves special attention since it is a prevailing tool for interface analysis that can be employed in real-time analysis of different physicochemical or electrochemical properties of the interfaces such as phase changes, morphological evolution, mechanical properties, volume expansion, and surface electrochemical activity and so on [41].

The SPM can be operated in different modes including from atomic force microscopy to electrochemical atomic force microscopy. The Kelvin probe force microscopy, scanning ion conductance microscopy electrochemical strain microscopy and scanning electrochemical microscopy, are yet another modifications of the SPM technique. The SPM can probe the interfacial dynamics such as, electrochemical parameters, ionic transport through the interface, and dynamics of diffusion, interfacial surface mappings, morphological changes in the interface, mechanical strain and degradation of the interface. The electrochemical processes that occur at the interfaces are in the nano-scale as mentioned earlier. Most of the probing instruments probe the dynamics of the materials at macroscale. This gives the room for SPM technique as a powerful tool for electrochemical characterizations.

Kelvin Probe Force Microscopy (KPFM) is a variant of Atomic Force Microscopy (AFM) in the peak force tapping mode and can be used as a tool to elucidate the electric potential dissemination across the interface region in ASSBs. Masuda et al. [42] used in-situ KPFM to characterize the variation in internal potential distribution of a composite cathode before and after charging. After charging, the potential increased in the composite cathode electrode, indicates the Li ions depletion that occur in the solid electrolyte region. The KPFM can measure the interfacial potential, and thus highly useful tool to estimate the interfacial charge transfer [42, 43].

The Electrochemical Strain Microscopy (ESM) is one of the innovative SPM technique, which can be employed to probe the diffusion and deformation of the electrode/electrolyte materials from the developed strain in the materials by the external bias voltage. In this method when the AC bias voltage that applied through the probe results in some redistribution of Li ions within the sample. This can be measured as the electrochemical strain from the surface of the sample using the same probe. If we want to measure the AC bias to a larger area, one can switch AC and DC bias probing simultaneously by using one Switching Spectroscopy with ESM (SS-ESM). The probes should be highly conductive for the precise measurements. Wang et al. explains the role of ESM and SS-ESM technique to elucidate the electrochemical strain developed in the $Li_{1.5}Al_{0.5}Ge_{1.5}(PO_4)_3$ (LAGP) solid electrolyte material. The electrochemical strain distribution analysis in LAGP shows that the strain developed at the grain boundary region is higher than that of the grain regions. The Fig. 8.7 portraits the schematic of the ESM techniques, topographic and electrochemical strain analysis in the LAGP solid electrolyte material. The study reports that the average electrochemical strain of electrode materials is ~3 pm and the LAGP electrolyte is about 6 pm within the grains and around 15 pm at the grain boundary [37, 38]. This technique can be properly scaled up to determine the strain developed on the surface of the solid electrolyte, electrodes, and its interfaces in ASSB assemblies. The electrochemical strain analysis will lead to explicate the reason for the development of high impedance that developed in ASSBs against the Li ion diffusion through the electrode, electrolyte, and interfaces.

All the interfacial phenomena are not reversible due to the formation of non-reversible SEI layers. The ESM technique fails to detect the volumetric strain developed due to cycling since the volume expansion is derived from the direct result of reversible electrochemical processes. This can be overcome by another technique called in-situ IVZ (current–voltage–impedance) spectroscopy which enables to probe the electrochemically irreversible processes [9, 44]. This technique uses the measurements of current, voltage and change in at the area of the probing tip. The SPM is considered as a powerful tool which can be extended to different modes since it can be integrated and can attach to different experimental conditions.

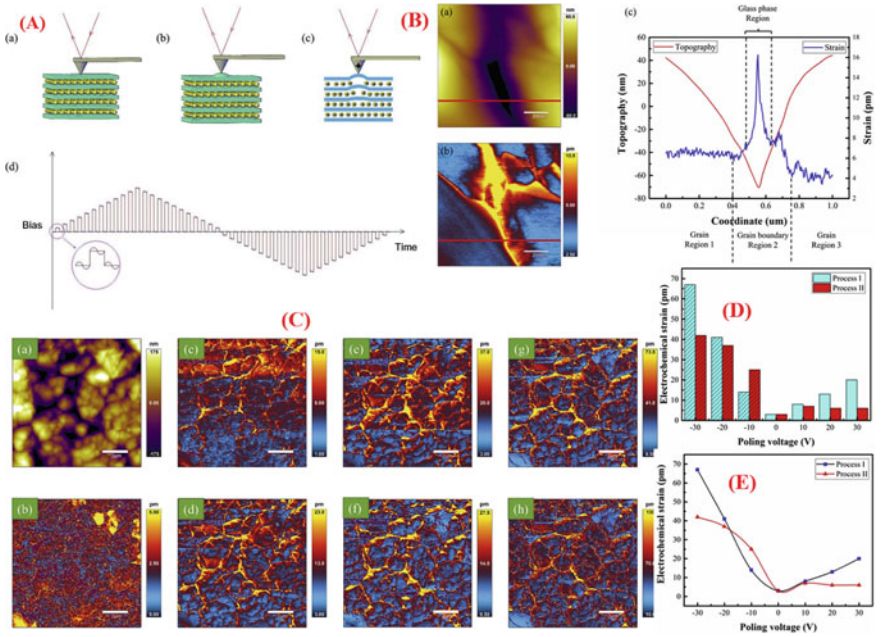

Fig. 8.7 The role of ESM and SS-ESM technique to elucidate the electrochemical strain developed in the $Li_{1.5}Al_{0.5}Ge_{1.5}(PO_4)_3$ (LAGP) solid electrolyte material; (**A**) The Schematic of: the ESM principle: (**a**) topography of the sample without tip bias, (**b**) with tip bias, (**c**) cross-section with tip bias, and (**d**) the principle of SS-ESM. (**B**) The ESM image of LAGP solid electrolyte: (**a**) topography, (**b**) electrochemical strain, and (**c**) a line analysis of topography and electrochemical strain.: (**a**) Topography and (**b–h**) ESM images in process I: (**b**) before poling, and poling by (**c**) +10 V, (**d**) +20 V, (**e**) +30 V, (**f**) −10 V, (**g**) −20 V and (**h**) −30 V, respectively.; (**D**) The bar chart (**a**) and line graph (**b**) of the average electrochemical strains in process I (in the order of +10: +20: +30, −10: −20 and −30 V DC voltage) and process II (in the order of −10: −20: −30, +10: +20 and +30 V). Reprinted from reference [37] with permission from Elsevier, Copyright © 2020

8.4 Conclusion and Future Research Perspectives

The solid–solid interfaces are considered as the key for the successful working of ASSBs. The interfacial resistance for the lithium-ion (Li ion) transfer between cathodes and solid electrolytes remains large in ASSBs. The interfacial resistance is initiated by the deviations in the chemical composition, at the interface region. The probing of ASSBs are limited by the lack of sophisticated instrumentations. To overcome the issues that impede the ion intercalation across the interface, it is critical to systematically understand the interface evolution in ASSBs. The decomposition of the solid electrolyte and side reactions that take place at the electrolyte–electrode interfaces, make it difficult to differentiate the composition of the interface that originated from different reactions after a few cycling. The development of new instruments to clearly elucidate the step by step formation/working of the ASSB interfaces are highly desired and need of the hour for the future development of the

ASSB industry. It would clue to the design and development of high-performance ASSBs.

Better knowledge on the atomic level structure and energetics that occurs in the interfaces is necessary to achieve systematic improvement of solid-state batteries with enhanced performance. Most of the solid-state electrolyte materials and its interfaces after cycling shows highly sensitive to moisture and atmospheric air. This makes the post-characterization of the interfaces becomes highly challenging, pointing to the significance of the sophisticated characterization techniques in in-situ and in-operando mode of analysis to unravel the interfacial mechanism in ASSBs [28].

One another challenge with the interfacial characterization technique is that the in-situ/operando techniques employed to analyze one system is usually not pertinent to the other systems. The clear understanding of the chemical reactions and phase transformations that befall at the solid–solid interface deserves dynamic analytical characterization of interfacial behavior [25]. This is considered to be priceless in crafting innovative ASSB assemblies with low interfacial impedance [25]. The comprehensive interface characterization tools helps to apprehend the potential of ASSB technology for a wide variety of forecasted and yet unforeseen dimensions for the next-generation societal needs.

Acknowledgements K. P. A. was supported by the European Structural and Investment Funds, OP RDE funded project 'CHEMFELLS IV' (No. CZ.02.2.69/0.0/0.0/20_079/0017899. Z. S. was supported by ERC-CZ program (project LL2101) from Ministry of Education Youth and Sports (MEYS).

References

1. Zhang, Z., Shao, Y., Lotsch, B., Hu, Y.-S., Li, H., Janek, J., Nazar, L.F., Nan, C.-W., Maier, J., Armand, M., Chen, L.: New horizons for inorganic solid state ion conductors. Energy Environ. Sci. **11**(8), 1945–1976 (2018). https://doi.org/10.1039/C8EE01053F
2. Miao, X., Wang, H., Sun, R., Wang, C., Zhang, Z., Li, Z., Yin, L.: Interface engineering of inorganic solid-state electrolytes for high-performance lithium metal batteries. Energy Environ. Sci. **13**(11), 3780–3822 (2020). https://doi.org/10.1039/D0EE01435D
3. Duan, J., Tang, X., Dai, H., Yang, Y., Wu, W., Wei, X., Huang, Y.: Building safe lithium-ion batteries for electric vehicles: a review. Electrochem. Energy Rev. **3**(1), 1–42 (2020). https://doi.org/10.1007/s41918-019-00060-4
4. Liang, Z., Zou, Q., Wang, Y., Lu, Y.-C.: Recent progress in applying in situ/operando characterization techniques to probe the solid/liquid/gas interfaces of Li–O_2 batteries. Small Methods **1**(7), 1700150 (2017). https://doi.org/10.1002/smtd.201700150
5. Li, Y., Zhang, D., Xu, X., Wang, Z., Liu, Z., Shen, J., Liu, J., Zhu, M.: Interface engineering for composite cathodes in sulfide-based all-solid-state lithium batteries. J. Energy Chem. **60**, 32–60 (2021). https://doi.org/10.1016/j.jechem.2020.12.017
6. Xiang, Y., Li, X., Cheng, Y., Sun, X., Yang, Y.: Advanced characterization techniques for solid state lithium battery research. Mater. Today **36**, 139–157 (2020). https://doi.org/10.1016/j.mattod.2020.01.018
7. Li, Y., Gao, Z., Hu, F., Lin, X., Wei, Y., Peng, J., Yang, J., Li, Z., Huang, Y., Ding, H.: Advanced characterization techniques for interface in all-solid-state batteries. Small Methods **4**(9), 2000111 (2020). https://doi.org/10.1002/smtd.202000111

8. Augustyn, V., McDowell, M.T., Vojvodic, A.: Toward an atomistic understanding of solid-state electrochemical interfaces for energy storage. Joule **2**(11), 2189–2193 (2018). https://doi.org/10.1016/j.joule.2018.10.014
9. Kempaiah, R., Vasudevamurthy, G., Subramanian, A.: Scanning probe microscopy based characterization of battery materials, interfaces, and processes. Nano Energy **65**, 103925 (2019). https://doi.org/10.1016/j.nanoen.2019.103925
10. Sångeland, C., Mindemark, J., Younesi, R., Brandell, D.: Probing the interfacial chemistry of solid-state lithium batteries. Solid State Ion. **343**, 115068 (2019). https://doi.org/10.1016/j.ssi.2019.115068
11. Koerver, R., Aygün, I., Leichtweiß, T., Dietrich, C., Zhang, W., Binder, J.O., Hartmann, P., Zeier, W.G., Janek, J.: Capacity fade in solid-state batteries: interphase formation and chemomechanical processes in nickel-rich layered oxide cathodes and lithium thiophosphate solid electrolytes. Chem. Mater. **29**(13), 5574–5582 (2017). https://doi.org/10.1021/acs.chemmater.7b00931
12. Auvergniot, J., Cassel, A., Ledeuil, J.-B., Viallet, V., Seznec, V., Dedryvère, R.: Interface stability of argyrodite Li_6PS_5Cl toward $LiCoO_2$, $LiNi_{1/3}Co_{1/3}Mn_{1/3}O_2$, and $LiMn_2O_4$ in bulk all-solid-state batteries. Chem. Mater. **29**(9), 3883–3890 (2017). https://doi.org/10.1021/acs.chemmater.6b04990
13. Wenzel, S., Weber, D.A., Leichtweiss, T., Busche, M.R., Sann, J., Janek, J.: Interphase formation and degradation of charge transfer kinetics between a lithium metal anode and highly crystalline $Li_7P_3S_{11}$ solid electrolyte. Solid State Ion. **286**, 24–33 (2016). https://doi.org/10.1016/j.ssi.2015.11.034
14. Doux, J.-M., Nguyen, H., Tan, D.H.S., Banerjee, A., Wang, X., Wu, E.A., Jo, C., Yang, H., Meng, Y.S.: Stack pressure considerations for room-temperature all-solid-state lithium metal batteries. Adv. Energy Mater. **10**(1), 1903253 (2020). https://doi.org/10.1002/aenm.201903253
15. Lee, Y.-G., Fujiki, S., Jung, C., Suzuki, N., Yashiro, N., Omoda, R., Ko, D.-S., Shiratsuchi, T., Sugimoto, T., Ryu, S., Ku, J.H., Watanabe, T., Park, Y., Aihara, Y., Im, D., Han, I.T.: High-energy long-cycling all-solid-state lithium metal batteries enabled by silver–carbon composite anodes. Nat. Energy **5**(4), 299–308 (2020). https://doi.org/10.1038/s41560-020-0575-z
16. Liu, X.H., Huang, J.Y.: In situ TEM electrochemistry of anode materials in lithium ion batteries. Energy Environ. Sci. **4**(10), 3844–3860 (2011). https://doi.org/10.1039/C1EE01918J
17. Williams, D.B., Carter, C.B.: The transmission electron microscope. In: Williams, D.B., Carter, C.B. (eds.) Transmission Electron Microscopy: A Textbook for Materials Science, pp. 3–17. Springer, US, Boston, MA (1996)
18. Reimer, L.: Scanning electron microscopy: physics of image formation and microanalysis, second edition. Meas. Sci. Technol. **11**(12), 1826–1826 (2000). https://doi.org/10.1088/0957-0233/11/12/703
19. Egerton, R.: Physical Principles of Electron Microscopy: An Introduction to TEM, SEM, and AEM. Springer, US (2011)
20. Tsai, C.-L., Roddatis, V., Chandran, C.V., Ma, Q., Uhlenbruck, S., Bram, M., Heitjans, P., Guillon, O.: $Li_7La_3Zr_2O_{12}$ interface modification for Li dendrite prevention. ACS Appl. Mater. Interfaces **8**(16), 10617–10626 (2016). https://doi.org/10.1021/acsami.6b00831
21. Kim, H.-S., Oh, Y., Kang, K.H., Kim, J.H., Kim, J., Yoon, C.S.: Characterization of sputter-deposited $LiCoO_2$ thin film grown on NASICON-type electrolyte for application in all-solid-state rechargeable lithium battery. ACS Appl. Mater. Interfaces **9**(19), 16063–16070 (2017). https://doi.org/10.1021/acsami.6b15305
22. Kato, T., Yoshida, R., Yamamoto, K., Hirayama, T., Motoyama, M., West, W.C., Iriyama, Y.: Effects of sintering temperature on interfacial structure and interfacial resistance for all-solid-state rechargeable lithium batteries. J. Power Sources **325**, 584–590 (2016). https://doi.org/10.1016/j.jpowsour.2016.06.068
23. Sakuda, A., Hayashi, A., Tatsumisago, M.: Interfacial observation between $LiCoO_2$ electrode and Li_2S–P_2S_5 solid electrolytes of all-solid-state lithium secondary batteries using transmission electron microscopy. Chem. Mater. **22**(3), 949–956 (2010). https://doi.org/10.1021/cm901819c

24. Nomura, Y., Yamamoto, K., Hirayama, T., Ohkawa, M., Igaki, E., Hojo, N., Saitoh, K.: Quantitative operando visualization of electrochemical reactions and Li ions in all-solid-state batteries by STEM-EELS with hyperspectral image analyses. Nano Lett. **18**(9), 5892–5898 (2018). https://doi.org/10.1021/acs.nanolett.8b02587
25. Wang, Z., Santhanagopalan, D., Zhang, W., Wang, F., Xin, H.L., He, K., Li, J., Dudney, N., Meng, Y.S.: In situ STEM-EELS observation of nanoscale interfacial phenomena in all-solid-state batteries. Nano Lett. **16**(6), 3760–3767 (2016). https://doi.org/10.1021/acs.nanolett.6b01119
26. Zhu, W., Liu, D., Paolella, A., Gagnon, C., Gariépy, V., Vijh, A., Zaghib, K.: Application of operando X-ray diffraction and Raman spectroscopies in elucidating the behavior of cathode in lithium-ion batteries. Front. Energy Res. **6**(66) (2018). https://doi.org/10.3389/fenrg.2018.00066
27. Yang, F., Liu, Y., Martha, S.K., Wu, Z., Andrews, J.C., Ice, G.E., Pianetta, P., Nanda, J.: Nanoscale morphological and chemical changes of high voltage lithium-manganese rich NMC composite cathodes with cycling. Nano Lett. **14**(8), 4334–4341 (2014). https://doi.org/10.1021/nl502090z
28. Li, X., Ren, Z., Norouzi Banis, M., Deng, S., Zhao, Y., Sun, Q., Wang, C., Yang, X., Li, W., Liang, J., Li, X., Sun, Y., Adair, K., Li, R., Hu, Y., Sham, T.-K., Huang, H., Zhang, L., Lu, S., Luo, J., Sun, X.: Unravelling the chemistry and microstructure evolution of a cathodic interface in sulfide-based all-solid-state Li-ion batteries. ACS Energy Lett. **4**(10), 2480–2488 (2019). https://doi.org/10.1021/acsenergylett.9b01676
29. Li, W., Li, M., Hu, Y., Lu, J., Lushington, A., Li, R., Wu, T., Sham, T.-K., Sun, X.: Synchrotron-based X-ray absorption fine structures, X-ray diffraction, and X-ray microscopy techniques applied in the study of lithium secondary batteries. Small Methods **2**(8), 1700341 (2018). https://doi.org/10.1002/smtd.201700341
30. Akita, Y., Segawa, M., Munakata, H., Kanamura, K.: In-situ Fourier transform infrared spectroscopic analysis on dynamic behavior of electrolyte solution on $LiFePO_4$ cathode. J. Power Sources **239**, 175–180 (2013). https://doi.org/10.1016/j.jpowsour.2013.03.134
31. Ogata, K., Salager, E., Kerr, C.J., Fraser, A.E., Ducati, C., Morris, A.J., Hofmann, S., Grey, C.P.: Revealing lithium–silicide phase transformations in nano-structured silicon-based lithium ion batteries via in situ NMR spectroscopy. Nat. Commun. **5**(1), 3217 (2014). https://doi.org/10.1038/ncomms4217
32. Prabu, M., Selvasekarapandian, S.: Dielectric and modulus studies of $LiNiPO_4$. Mater. Chem. Phys. **134**(1), 366–370 (2012). https://doi.org/10.1016/j.matchemphys.2012.03.003
33. Croce, F., Scrosati, B.: Interfacial phenomena in polymer-electrolyte cells: lithium passivation and cycleability. J. Power Sources **43**(1), 9–19 (1993). https://doi.org/10.1016/0378-7753(93)80097-9
34. Abhilash, K.P., Christopher Selvin, P., Nalini, B., Jose, R., Vijayaraghavan, R., Chowdari, B.V.R., Adams, S., Reddy, M.V.: Investigations on the influence of Sm^{3+} ion on the nano TiO_2 matrix as the anode material for lithium ion batteries. J. Alloy. Compd. **710**, 205–215 (2017). https://doi.org/10.1016/j.jallcom.2017.03.094
35. Abhilash, K.P., Selvin, P.C., Nalini, B., Jose, R., Hui, X., Elim, H.I., Reddy, M.V.: Correlation study on temperature dependent conductivity and line profile along the LLTO/LFP–C cross section for all solid-state Lithium-ion batteries. Solid State Ion. **341**, 115032 (2019). https://doi.org/10.1016/j.ssi.2019.115032
36. Richards, W.D., Miara, L.J., Wang, Y., Kim, J.C., Ceder, G.: Interface stability in solid-state batteries. Chem. Mater. **28**(1), 266–273 (2016). https://doi.org/10.1021/acs.chemmater.5b04082
37. Wang, Z., Kotobuki, M., Lu, L., Zeng, K.: Nanoscale characterization of solid electrolyte by scanning probe microscopy techniques. Electrochim. Acta **334**, 135553 (2020). https://doi.org/10.1016/j.electacta.2019.135553
38. Yang, S., Yan, B., Wu, J., Lu, L., Zeng, K.: Temperature-dependent lithium-ion diffusion and activation energy of $Li_{1.2}Co_{0.13}Ni_{0.13}Mn_{0.54}O_2$ thin-film cathode at nanoscale by using electrochemical strain microscopy. ACS Appl. Mater. Interfaces **9**(16), 13999–14005 (2017). https://doi.org/10.1021/acsami.6b16321

39. He, Y., Lu, C., Liu, S., Zheng, W., Luo, J.: Interfacial incompatibility and internal stresses in all-solid-state lithium ion batteries. Adv. Energy Mater. **9**(36), 1901810 (2019). https://doi.org/10.1002/aenm.201901810
40. Binnig, G., Rohrer, H.: Scanning tunneling microscopy. Surf. Sci. **126**(1), 236–244 (1983). https://doi.org/10.1016/0039-6028(83)90716-1
41. Strelcov, E., Yang, S.M., Jesse, S., Balke, N., Vasudevan, R.K., Kalinin, S.V.: Solid-state electrochemistry on the nanometer and atomic scales: the scanning probe microscopy approach. Nanoscale **8**(29), 13838–13858 (2016). https://doi.org/10.1039/C6NR01524G
42. Masuda, H., Ishida, N., Ogata, Y., Ito, D., Fujita, D.: Internal potential mapping of charged solid-state-lithium ion batteries using in situ Kelvin probe force microscopy. Nanoscale **9**(2), 893–898 (2017). https://doi.org/10.1039/C6NR07971G
43. Zhu, J., Zeng, K., Lu, L.: In-situ nanoscale mapping of surface potential in all-solid-state thin film Li-ion battery using Kelvin probe force microscopy. J. Appl. Phys. **111**(6), 063723 (2012). https://doi.org/10.1063/1.3699214
44. Yang, S.M., Strelcov, E., Paranthaman, M.P., Tselev, A., Noh, T.W., Kalinin, S.V.: Humidity effect on nanoscale electrochemistry in solid silver ion conductors and the dual nature of its locality. Nano Lett. **15**(2), 1062–1069 (2015). https://doi.org/10.1021/nl5040286